Chapter 14

Electrocatalytic Applications of Graphene–Metal Oxide Nanohybrid Materials

Arnab Halder, Minwei Zhang and Qijin Chi

Additional information is available at the end of the chapter

http://dx.doi.org/10.5772/61808

Abstract

Development of state-of-the-art electrocatalysts using commercially available precursors with low cost is an essential step in the advancement of next-generation electrochemical energy storage/conversion systems. In this regard, noble metal-free and graphene-supported nanocomposites are of particular interest. Graphene-based nanocomposite is an excellent candidate as energy-device and sensor-related electrode materials, largely due to their high electrical conductivity, large specific surface area, high-speed electron/heat mobility, and reasonably good mechanical strength. Among many types of graphene-based composite materials, graphene–metal oxide nanohybrids hold great promise toward engineering efficient electrocatalysts and have attracted increasing interest in both scientific communities and industrial partners around the world. The goal of this chapter is primarily set on an overview of cutting-edge developments in graphene–metal oxide nanohybrid materials, with the recently reported results from worldwide research groups. This chapter is presented first with an introduction, followed by synthetic methods and structural characterization of nanocomposites, an emphasis on their applications in energy and sensor-related fields, and finally completed with brief conclusions and outlook.

Keywords: Graphene, metal oxides, graphene–metal oxide nanohybrids, electrocatalysis, energy storage and conversion, sensors, electrochemistry

1. Introduction

Graphene, a single atomic thick layer of graphite with closely packed conjugated and hexagonally connected carbon atoms, has attracted tremendous attention since its discovery in 2004 because of its large specific surface area, high-speed electron mobility, good mechanical strength, high electric and thermal conductivity, room temperature quantum hall effect, good

optical transparency, and tunable band gap [1, 2]. This material has a theoretical surface area of 2630 $m^2 g^{-1}$, a mobility of 200,000 $cm^2 V^{-1} s^{-1}$ at a carrier density of ~10^{12} cm^{-2}, and the highest electrical conductivity of 106 s cm^{-1} at room temperature [3, 4]. Also, graphene has a Young's modulus of ~1 TPa, breaking strength of 42 N m^{-1} [5], and thermal conductivity of 5000 W $m^{-1} K^{-1}$ [6]. For all these versatile properties and obvious advantages, a rapid development of graphene-based materials has been witnessed in the fields of chemistry, physics, biology, and many other interdisciplinary fields such as nanotechnology and nanomedicine.

Electrocatalysis is a special type of catalysis that speeds up the rate of an electrochemical reaction occurring on electrode surfaces or at liquid/solid interfaces. Various kinds of electrochemical reactions are involved for different electrocatalytic applications in energy and sensor-related fields. Therefore, design and fabrication of advanced electrocatalysts with outstanding performance and low cost are of great significance for the commercialization of electrocatalytic-system-based energy devices. Metal oxide nanostructures have been identified as one of the most important electrocatalytic materials due to their several advantages. *Firstly*, they have exceptional electrical, optical, and molecular properties. *Secondly*, there is further possibility to insert more functional groups on the surface for the immobilization of other biological catalysts. *Thirdly*, metal oxides have higher alkaline corrosion resistance compared to other materials in electrochemical environmental due to the stabilization of the higher oxidation state of the transition metals. *Finally*, their unique crystalline structures benefit in preventing the agglomeration of metal oxide nanostructures with their size retained [7]. Besides electrocatalytic activity and cost, the stability and durability of a catalyst are very critical issues for practical applications. In addition, a good catalyst support is needed, which should have a large surface area for catalyst dispersion, excellent electronic conductivity, and high electrochemical stability in different electrolytes. In recent years, various catalyst support materials have been proposed and studied. In this regard, graphene nanosheets have shown promising characteristics for wide applications as 2D support materials for different electrocatalysts. In the last decade, intensive efforts have been devoted to functionalize graphene-based nanomaterials and to explore their applications in sensors [8],[9], electrochemical energy storage [10, 11], electronics, optoelectronics [12], and others. Graphene-based nanocomposites provide a new option as electrode materials in the field of electrocatalytic applications due to their high electrical conductivity, high surface area, and richness of functional groups for further modification. The rapid development of low cost and facile preparation methods of graphene-based nanocomposites has promoted their practical industrial applications. The catalytic activity of the graphene-supported catalysts can be improved, due to enhanced electronic communication (e.g., charge transfer) between catalysts and support. Furthermore, arising from their synergistic effects of graphene sheets and functionalized components, the nanocomposites can offer novel physicochemical properties and consequently improve electrochemical performances. As a result, graphene-based nanocomposites have thus been regarded as one of the most promising hybrid materials that can drive the development of more efficient next-generation energy devices as well as applied in the fabrication of electrochemical and gas sensors. This chapter is focused on one of such nanocomposites, made of chemically exfoliated graphene and metal oxides. We overview and discuss their synthesis methods, structural features, electrocatalytic applications, and future perspectives.

http://dx.doi.org/10.5772/61808

2. Synthesis of graphene–metal-oxide-based nanohybrid composites

2.1. Introduction

In terms of electrocatalysis, graphene-supported metal oxides nanohybrid materials have exhibited promising applications because of the following well-recognized advantages. *Firstly*, the large surface area and 2D flexibility of graphene nanosheets can offer sufficient space to accommodate different nanomaterials and also prevent their agglomeration. *Secondly*, due to the good superficial characteristics of graphene, solid-air contact efficiency increases and simultaneously the amount of oxygen adsorption also increases. *Thirdly*, the electrical conductivity of graphene promotes the electron transfer rate on the surface. *Finally*, the structural defects of graphene also provide more active sites for further modification with different functional groups to promote the selective electrocatalysis.

Incorporation of inorganic nanomaterial onto the surface of graphene has attracted tremendous attention for the development of new-generation catalytic materials [13]. These novel nanostructures show superior electrocatalytic activity, selectivity, and long-term stability, which can serve as promising electrode material for different electrochemical reactions. Different metal oxides are promising in this regard for the replacement of noble-metal-based electrocatalysts. But normally metal oxides are poorly conductive and often suffer from dissolution and aggregation during the electrochemical reactions [14, 15]. It was proposed that anchoring metal oxide nanostructures onto graphene surface by suitable synthetic procedure could solve the problems. Indeed, some graphene-supported metal oxide nanocomposites have displayed remarkable improvements in electrocatalytic activity and stability toward some crucial electrochemical reactions in amperometric sensors and energy storage and conversion.

2.2. Major synthetic methods

The increasing interest in graphene-based metal oxides nanohybrid materials for different electrocatalytic applications has led to a variety of new processes proposed for the synthesis of nanocomposite materials. Some recently established methods are discussed in this section.

2.2.1. Solvothermal and hydrothermal synthetic approaches

Solvothermal and hydrothermal synthetic approaches are one of the most common synthetic strategies for the development of different graphene-based nanohybrid electrocatalysts. Song et al. [16] reported a new hydrothermal approach for the preparation of CuO/GO nanocomposite materials, which used cupric acetate and graphene oxide as precursors. The reaction was conducted for 10 h under different temperatures (120, 150, and 180°C). The final product was washed by deionized water and dried for the electrocatalytic applications. Dong et al. [17] introduced another hydrothermal approach for the preparation of Graphene/Co_3O_4 nanowire composite. They used presynthesized 3D graphene and $CoCl_2.6H_2O$ as starting materials. This reaction was proceeded in autoclave at 120°C for 16 h. Dai et al. [18] also used a hydrothermal approach for the synthesis of covalent hybrid of spinel manganese–cobalt oxide and graphene.

They employed a two-step procedure to synthesize $MnCo_2O_4$–graphene oxide nanohybrids. In the first nucleation step, $Co(OAc)_2$ and $Mn(OAc)_2$ were mixed at 80°C with mildly oxidized graphene oxide in an ethanol/water NH_4OH solution. In the second step, hydrothermal treatment was done at 150°C to achieve the nitrogen-doped graphene. And the final material showed an excellent electrocatalytic activity for oxygen reduction reaction (ORR). Dai et al. [19] also used cobalt acetate and GO as a precursor for the hydrothermal synthesis of Co_3O_4/graphene hybrid bifunctional catalyst for ORR and water oxidation or oxygen evolution reaction (OER).

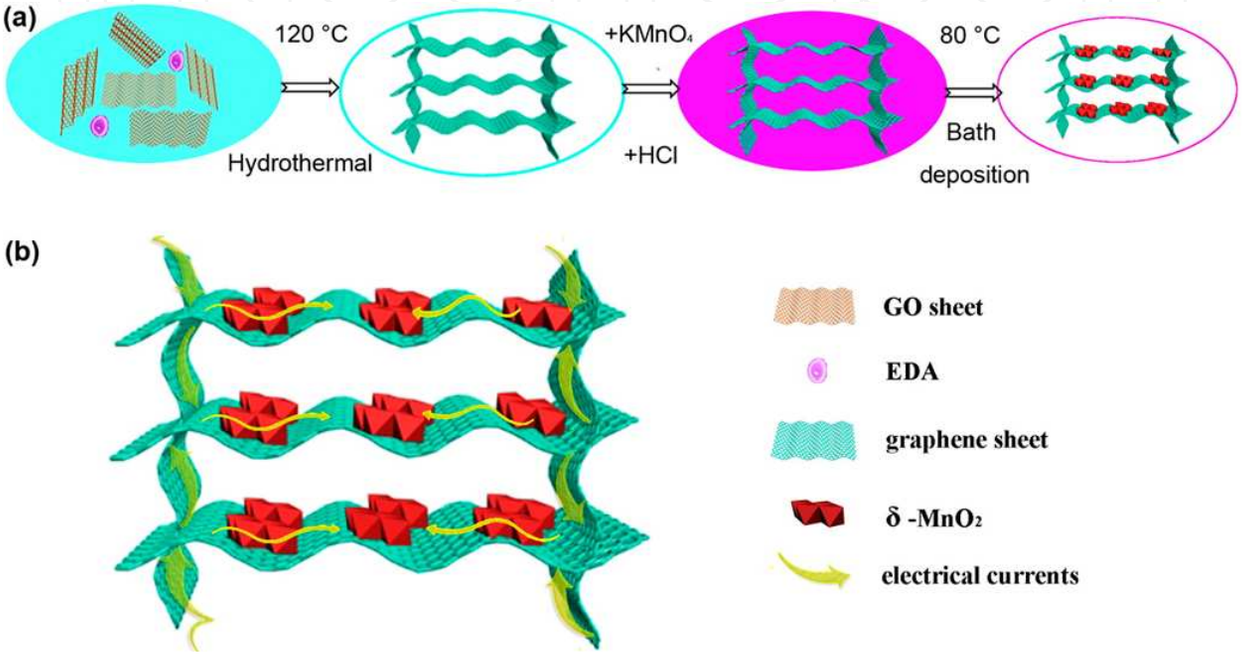

Figure 1. Schematic illustration of the hydrothermal synthesis of 3D graphene/MnO_2 (a), and schematic illustration of electrons transfer on the 3D hybrid material (b). (Reproduced with permission from ref. 44 Copyright 2014 American Chemical Society)

Wang et al. [20] reported a hydrothermal approach for the synthesis of CoO/rGO nanocomposite using GO, Co $(Ac)_2.4H_2O$, $Co(NH_2)_2$ as a precursor (190°C, 2 h). Mullen et al. [21] successfully synthesized 3D nitrogen-doped graphene aerogel-supported Fe_3O_4 nanoparticles by hydrothermal approach for the efficient electrocatalysis of ORR. Graphene oxide, iron acetate, and polypyrrole were hydrothermally assembled at 180°C for 12 h to form a 3D graphene-based hydrogel. The hydrogel was further dehydrated and annealed at 600°C for 3 h under nitrogen atmosphere.

Hydrothermal methods for the synthesis of graphene-based hybrid materials can be carried out at different temperature ranges, up to 190°C [22]. Figure 1 shows an example for the preparation of 3D graphene–MnO_2 composites. There are several advantages of using hydrothermal process. *Firstly*, the strong electrolyte water possesses a high diffusion coefficient and dielectric constant under hydrothermal reaction conditions, which helps to remove the oxygen-containing groups via dehydration and also accelerates heterolytic bond cleavage.

Secondly, this is a green reduction approach and does not add any further impurities to the final product. *Thirdly*, the degree of reduction and the properties of the hybrid material can be tuned by adjusting temperature and pressure of the reaction. And *finally*, the process could be easily implemented in an industry scale with a relatively simple setup (an autoclave) and low cost. A possible disadvantage of the method could be the consumption of significant amount of energy.

2.2.2. Chemical reduction approaches

Chemical reduction is another method among the most common approaches for the preparation of different graphene-based nanohybrid electrocatalysts. Different research groups have used different types of reducing agents for the specific synthesis purposes. For example, Qiao et al. [23] reported a simple chemical reduction method for the preparation of CuO/N-rGO nanohybrid using NaOH in the mixture of $CuCl_2$ and N-doped reduced graphene oxide. Guo et al. [24] used diethylene glycol (DEG) as a reducing agent for the preparation of Cu_2O/RGO composite material. Yang et al. [25] prepared PDDA-G/Fe_3O_4 nanohybrid material using ammonia solution as a reducing agent. Khezrian et al. [26] also used ammonia solution as a reducing agent for the synthesis of Fe_3O_4 magnetic nanoparticles/RGO hybrid nanosheets. Wang et al. [27] used citric acid for the preparation of MnO_2/GO. Ruoff et al. [28] used hydrazine as a reducing agent for the synthesis of RGO/tin oxide (TiO_2) nanocomposite.

The major advantage of this approach is that one can tune the degree of reduction and other properties by using specific reducing agents. And also for most of cases the reactions are very energy-efficient due to low temperatures and slow time. An obvious drawback is the need of purifying the final product from different reducing agents, which is in some cases quite challenging.

2.2.3. MW-assisted synthetic approaches

Microwave (MW)-assisted synthesis is a simple and popular technique for the fast production of nanomaterials with small particle dimensions, uniform particle size distribution, and high purity. It is a uniform heating procedure compared to the other conventional heating systems. Moreover, microwave can facilitate the nucleation of nanoparticles and shorten the synthesis time. There are some excellent examples of using this approach. For instance, Peng et al. [29] synthesized CuO/SG hybrid materials by MW-assisted method using graphene oxide and cupric acetate as a precursor (Fig. 2). Ruoff et al. [30] also reported MW-assisted method for the synthesis of RGO/Fe_2O_3. Ferric chloride and graphene oxide were used as precursors for this method. And the as-synthesized nanocomposite was used as a high-performance anode material for lithium ion batteries. Wang et al. [31] synthesized highly dispersed titanium dioxide (TiO_2) nanoclusters on RGO in a toluene–water system by MW-irradiation-assisted method. The main advantages for the MW-assisted synthetic approaches include rapid reaction time, possibility for scale-up production and impurity-free final nanohybrid product. The relatively high cost needed for experimental setups could be a major drawback.

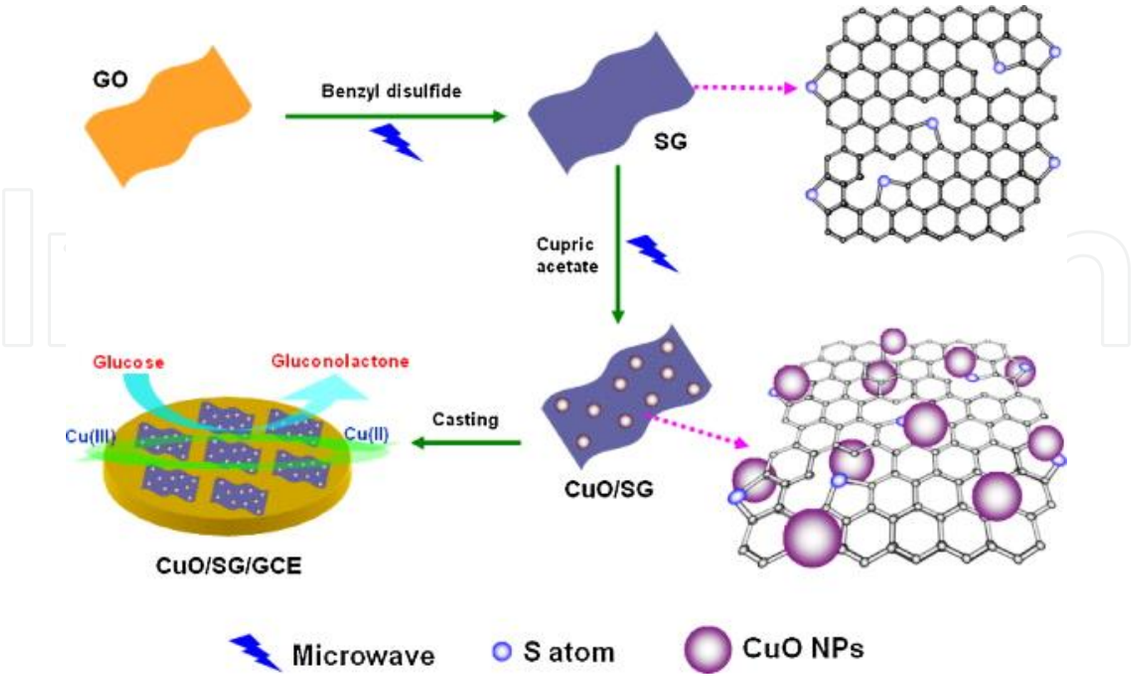

Figure 2. Schematic illustration of the MW-assisted synthesis of CuO nanoparticle supported on S-doped graphene/SG and CuO/SG on glassy carbon electrode for glucose sensing. (Reproduced with permission from ref. 29 Copyright Elsevier 2015)

2.2.4. Electrochemical synthetic approaches

The electrochemical synthetic method is an efficient technique for transforming electronic states by regulating the external power source to change the Fermi energy level of the electrode material surface [32]. Kong et al. [33] successfully prepared CuO nano needle/graphene/carbon nanofiber modified electrodes by electrochemical synthetic approaches for nonenzymatic glucose sensing in saliva. Duan et al. [34] reported a novel electrochemical approach to deposit MnO_2 nanowires on graphene for the sensor applications. The MnO_2 nanowires were anodically electrodeposited onto a graphene paper electrode using a CV technique in the potential range from 1.4 V to 1.5 V with a scan rate of 250 mV s^{-1} (Fig. 3) by cyclic voltametry.

The electrochemical synthetic approach is a fast, controllable, and green technique. By this procedure, one can achieve impurity-free nanohybrid material using little power consumption. However, this approach normally yields solid nanocomposite products, which is difficult for further processing. And also it would be difficult for large-scale production.

2.2.5. Other synthetic approaches

There are several other techniques that have also been explored for the synthesis of different nanocomposites, such as electrospinning, template-based synthesis, light- or radiation-induced methods, etc. However, although among them each technique has its specific advantages for specific systems; to date, few have been widely used.

http://dx.doi.org/10.5772/61808

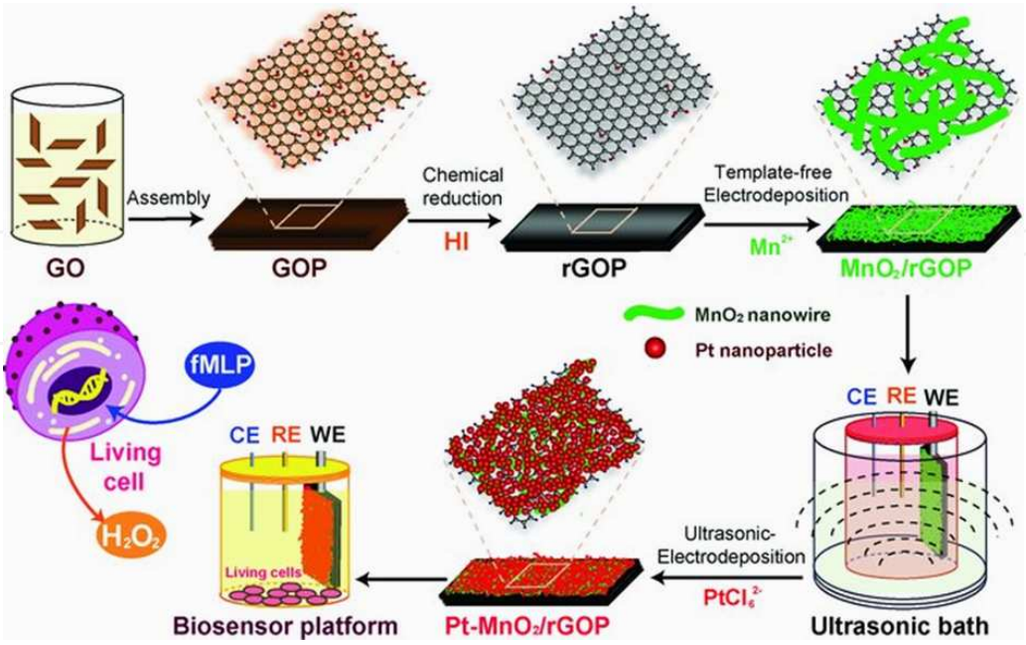

Figure 3. Schematic illustration of electrodeposition-assisted synthesis of MnO_2 nanoparticle supported on reduced graphene oxide paper electrode for biosensor applications. (Reproduced with permission from ref. 34 Copyright 2012 WILEY-VCH Verlag GmbH & Co. KGaA, Weinheim)

In summary, a number of methods have been developed for the synthesis of metal oxide/graphene composites, among which hydrothermal procedures have been most extensively used in particular. However, each method has its advantages as well as disadvantages. Table 1 summarizes the preparation methods and their major applications of most studied metal oxide/graphene nanocomposites.

Metal oxides	Nanohybrid electrocatalyst	Preparation method	Precursors	Applications	Ref
Copper oxide	RGO-Cu_2O	Heat treatment and sonication	GO, $CuSO_4.5H_2O$, $[C_{16}MMIm]Br$	Nonenzymatic amperometric glucose sensing	[35]
	CuNiO-graphene	Hydrothermal synthesis	$CuCl_2$, $NiCl_2$, Graphene	Nonenzymatic glucose sensors	[36]
	Cu_2O–rGO	Physical adsorption, in situ reduction and one pot synthesis	GO, $CuSO_4.5H_2O$, PDDA	Nonenzymatic H_2O_2 sensing	[37]
	CuO/ rGO/ CNF	Electrodeposition	GO, $CuCl_2$, carbon nanofiber	Nonenzymatic sensing of glucose in saliva	[33]

Metal oxides	Nanohybrid electrocatalyst	Preparation method	Precursors	Applications	Ref
	CuO/graphene	Heat treatment and annealing	Copper nitrate, GO	Nonenzymatic glucose sensors	[38]
	CuO/GO	Hydrothermal synthesis	GO, Cupric acetate, DMF	Nonenzymatic glucose sensors	[16]
	Cu_2O/GNs	Ultrasonication, stirring	GO, $CuCl_2$	Nonenzymatic H_2O_2 and glucose sensing	[39]
	CuO/SG	microwave-assisted solvothermal method	GO, Benzyl disulfide, Cupric acetate	Nonenzymatic glucose sensors	[29]
	CuO/N-rGO	Chemical reduction	N-rGO, $CuCl_2$	Direct methanol fuel cells	[23]
	Cu_2O/RGO	Chemical reduction	GO, Cupric acetate, DEG	Alkaline ORR	[24]
Cobalt oxide	Co_3O_4 /graphene	Ultrasonication and pyrolyzation	GO, cobalt phthalocyanine	Anode Materials for Li- Ion Batteries	[40]
	3D graphene/ Co_3O_4	Hydrothermal synthesis	Graphene, $CoCl_2.6H_2O$	Supercapacitors and enzymeless glucose sensors	[17]
	$MnCo_2O_4$/N-rGO	Hydrothermal method	GO, $Co(OAc)_2$, $Mn(OAc)_2$, NH_4OH	Alkaline ORR	[18]
	Co_3O_4/rmGO	Hydrothermal synthesis	GO, $Co(OAc)_2$, NH_4OH	Alkaline ORR	[19]
	CoO/CG	Aerosolization/ high-temperature	GO, $CoCl_2$	Enzymeless glucose sensors	[41]
	CoO/rGO	Hydrothermal synthesis	GO, Co $(Ac)_2$. $4H_2O$, $CO(NH_2)_2$	Electrochemical nonenzymatic sensor	[20]
Iron oxide	RG-O/Fe_2O_3	Microwave irradiation	GO, $FeCl_3$, N_2H_4	Anode Materials for Li- Ion Batteries	[30]
	RGO/Fe_3O_4	Chemical coprecipitation method	GO, $FeCl_3.6H_2O$, $FeCl_2.4H_2O$, NH_4OH	Nonenzymatic H_2O_2 sensing	[42]
	PDDA-G/Fe_3O_4	Chemical reduction	GO, $FeCl_3.6H_2O$, $FeSO_4$, PDDA	Amperometric H_2O_2 sensing	[25]
	Fe_3O_4/r-GO	Chemical reduction	GO, $FeCl_3.6H_2O$, $FeCl_2.4H_2O$	Eletrochemical NADH sensors	[26]
	3D Fe_3O_4/ N-GAs	Hydrothermal/ heat treatment	GO, iron(III) acetate, polypyrrole	Alkaline ORR	[43]

http://dx.doi.org/10.5772/61808

Metal oxides	Nanohybrid electrocatalyst	Preparation method	Precursors	Applications	Ref
Manganese oxide	MnO_2 /rGOP	Electrodeposition	GO, $MnSO_4$	Nonenzymatic H_2O_2 sensing	[34]
	GO/MnO_2	Chemical reduction	GO, $KMnO_4$	Nonenzymatic H_2O_2 sensing	[27]
	GO/MnO_2	Solution process	GO, MnO_2	Voltammetric sensor for hydroquinone and catechol	[44]
	PtAu–MnO_2/ GP	Electrodeposition	GO, $MnSO_4$	Nonenzymatic glucose sensors	[45]
	MnO_2/3D rGO	Chemical reduction	GO, $KMnO_4$	Electrochemical energy storage	[46]
	Mn_3O_4/GO	Hydrothermal method	GO, N_2H_4, $KMnO_4$	Alkaline ORR	[47]
	GO-MnO_2	Electrodeposition	GO, MnO_2	Alkaline ORR	[48]
Nickel oxide	NiONPs/GO	Electrodeposition	GO, $Ni(NO_3)_2.6H_2O$	Supercapacitor and enzymeless glucose sensors	[49]
	NA/NiONF-rGO	Electrospinning	GO, $C_4H_6O_4Ni.4H_2O$	Nonenzymatic glucose sensor	[50]
	NiO-GR	Electrodeposition	GO, $NiSO_4$	Nonenzymatic glucose sensor	[51]
Tin oxide	RG-O/SnO_2	Chemical reduction	GO, $SnCl_4.6H_2O$	Anode Materials for Li- Ion Batteries	[28]
	SnO_2-rGO	Hydrothermal method	GO, $SnCl_4.6H_2O$	NO_2 sensors	[52]
Titanium dioxide	RGO–TDN	Microwave synthesis	GO, titanium (IV) isopropoxide	Glucose sensors	[31]
	TiO_2-graphene	Hydrothermal method	GO, titanium (IV) isopropoxide	Adenine and Guanine sensors	[53]
	GN/TiO2	Template-based synthesis, Calcination	GO, titanium (IV) isopropoxide, CTAB	Determination of trace colorants in foods	[54]
	TiO_2@TiO_xN_y/TiN-GS	Hydrothermal/heat treatment	GO, TiO_2	Anode Materials for Li- Ion Batteries	[55]
	TiO_2-FGS	Chemical reduction	$TiCl_3$, CNT	Li- Ion Batteries	[56]
	TiO_2-FGS	Heat treatment	GO, sodium dodecyl sulfate (SDS), $TiCl_3$	Alkaline ORR	[57]

Metal oxides	Nanohybrid electrocatalyst	Preparation method	Precursors	Applications	Ref
Vanadium oxide	Graphene/ V_2O_5	Chemical reduction	GO, vanadyl tri isobutoxide	High-performance cathodes in Li-Ion batteries	[58]
	V_2O_5/GO	Chemical reduction, freeze drying	GO, HVO_3	Li-ion batteries	[59]
	3D VO_2 NR/ rGO	Hydrothermal/heat treatment	V_2O_5, GO	High-capacity supercapacitor electrodes	[60]
Zinc Oxide	Graphene/ZnO	Hydrothermal method	$ZnCl_2$, Graphene	Supercapacitors and electrochemical sensors	[61]
	rGO quantum dots/ZnO	Electrospinning	GO, ZnO	Intracellular H_2O_2 sensors	[62]

Table 1. Summary of the main synthetic methods for preparation of metal oxide–graphene nanocomposites and their major applications.

3. Structural characterization and physicochemical properties of graphene–metal oxide nanocomposites

As the synthesized graphene–metal oxide nanohybrid materials have tremendous effects on electrocatalytic applications, structural characterization is of paramount importance for understanding the correlation between their nanostructures and catalytic activity. The fundamental knowledge about the structural features of a nanocomposite is also essential for the building up of catalysts with optimal electrocatalytic activity. These structural features also offer helpful clues for further modification of the catalysts. In this section, we briefly summarize characterization of the structural features of different graphene–metal oxide nanocomposites by various instrumental techniques. These widely used techniques include scanning electron microscopy (SEM), transmission electron microscopy (TEM), atomic force microscopy (AFM), Raman spectroscopy, Fourier transform infrared spectroscopy (FTIR), X-ray photoelectron spectroscopy (XPS), energy dispersive X-ray spectroscopy (EDX), and thermogravimetric analysis (TGA).

3.1. Microscopic imaging of chemically exfoliated graphene and composites

The atomic structural features of a material affect its electronic, chemical, and catalytic properties. Various microscopic imaging techniques such as SEM, TEM, and AFM are proven as very essential tools to characterize nanomaterials. Their high-resolution capability enables to provide detailed information regarding shape, size, chemical composition, and phase of

http://dx.doi.org/10.5772/61808

nanomaterials. As a typical example, it has been well-shown that particle size, morphology, and exposed active facets have significant impacts on the catalytic efficiency of metal or metal oxide nanomaterials toward ORR electrocatalysis.

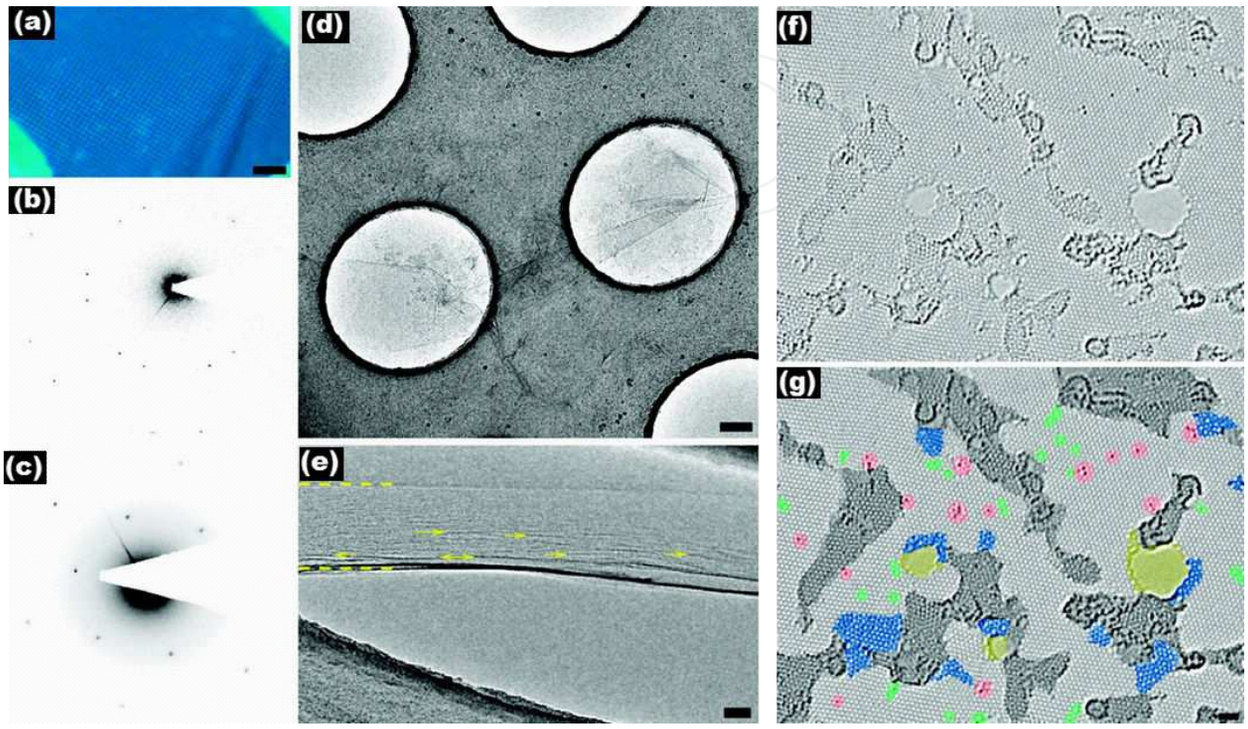

Figure 4. (a) Optical micrograph of graphene oxide sheets on the Quantifoil (QF) TEM grid. (b) Electron diffraction pattern of a bilayer area, displaying the stacking structure of the sheets. (c) Diffraction pattern from a single layer. (d) TEM image of RGO sheets on the QF grid. (e) TEM image with the sample tilted to 60°. The region between the horizontal dashed lines is a single layer (region above is a double layer, below is vacuum). Arrows indicate horizontal dark lines where the RGO sheet appears parallel to the beam, indicating local deformations up to 30°. Scale bars are 10 μm (a), 200 nm (d), and 10 nm (e). (f) Atomic resolution, aberration-corrected TEM image of a single layer reduced graphene oxide membrane. (g) Highlight with color in different areas. The light-gray color indicates the defect-free crystalline graphene area. Dark-gray shaded regions show the contaminated area. Blue regions indicate the disordered single-layer carbon networks, or extended topological defects due to the remnants of the oxidation–reduction process. Red areas indicate individual ad-atoms or substitutions. Green areas highlight isolated topological defects, that is, single bond rotations or dislocation cores. Holes and their edge reconstructions are marked in yellow color. Scale bar in (f) and (g) is 1 nm. (Reproduced with permission from ref. 65. Copyright ACS 2010)

SEM is mainly used to get the overall morphology of nanocomposites at large scales from several microns to 500 nm. However, to get more detailed and descriptive view of metal oxide nanocomposites and the crystal lattices or defects on graphene sheets, TEM and high-resolution TEM (HRTEM) are the most appropriate tools [63, 64]. The working principles of HRTEM are based on the interference of different transmitted and diffracted electron beams for building an image that can show the variation in phase. This is quite different from other traditional microscopic techniques, where sample image is derived from the variation of beam amplitudes due to the absorption of specimens. Compared to mechanically exfoliated graphene, the chemically synthesized graphene contains notable structural defects, but they could hardly be detected by normal spectroscopic and microscopic characterizations. TEM is one of

the leading methods for atomic scale imaging of graphene-based materials. For example, Fig. 4a shows an optical micrograph of RGO-coated Quantifoil (QF) TEM grid with the coverage visible as grayish spots [65]. TEM imaging analysis of the sample (Fig. 4d) showed that only ~1% of the holes of the whole grid were covered with sheets. Diffraction analysis was done to find holes covered by single-layered graphene sheets, which exhibited only one hexagonal pattern (Fig. 4c). These hexagonal patterns indicate the presence of a long-range hexagonal order orientation in the graphene sheets. Figure 4b indicates the parallel-beam diffraction pattern from a bilayer area, where two hexagonal patterns can be clearly detected. Then, the sample imaging was done under a high tilt (60°, Fig. 4e), which showed a high level of roughness, much more than that in mechanically exfoliated graphene sheets. The horizontal dark lines in Fig. 4e (arrows) was explained as representing the graphene layer in parallel to the electron beam. This image interprets that the wrinkles might be due to solution processing and drying, to stress, or to form defects in RGO. The high-resolution imaging of single-layered graphene sheets showed the actual atomic structure of the RGO layers, as represented in Figs. 4f and 4g. Various regions of the image are highlighted by colors in Fig. 4g. It is clearly observed that the largest part of the layer is formed of clean well-crystallized graphene areas where the hexagonal lattice is clearly seen (light-gray color in Fig. 4f). The visible well-crystallized areas are around 3–6 nm in the domain size and they cover ~60% of the whole plane. However, it is impossible to determine the exact structure of graphene with the adsorbed contamination, which covers ~30% of the total area. As most of the contaminants prefer to stick on the defects, the part of the defective areas is most likely underestimated. In spite of the presence of such a significant number of topological defects, the long-range oriented order of RGO is maintained. But such defects were normally not seen in any mechanically exfoliated graphene samples. Because the RGO and mechanically cleaved graphene samples were prepared from the same graphite source, it can be ruled out that the defects were from the starting material. These observations suggest that the high density of topological defects in these samples were introduced during graphene exfoliation by strong chemical oxidation and reduction. Although HRTEM can magnify the micro view into 1 nm, there is still limitation at around 0.2 nm. And, as electron beam heating can destroy small nanoparticles, the possibility of particle melting should be considered.

Song et al. [66] reported an alternative important strategy using scanning transmission electron microscopy (STEM), which combines the advantages of SEM and TEM and has extensively used in characterization of morphology and crystal structures of nanomaterials. Scanning probe microscopy techniques such as AFM and scanning tunneling microscopy (STM) also play an important role in the structural characterization of material surfaces with atomic resolution. Although the theoretical thickness of monolayer graphene is approximately 0.34 nm, the detected thickness by AFM analysis of a single layer of chemically synthesized GO is around 0.6–1.2 nm [67]. Although AFM can partially provide information regarding the number of layers in graphene, it is always better to associate it with Raman and XPS measurements for a complete chemical information. In addition, the STEM technique is also very helpful to obtain the lattice structure, surface morphology, particle size, and distribution of graphene-based materials surface at atomic resolution [68],[69],[70]. Figure 5a shows an overview of blue-shaded and uniformly folded graphene nanosheets taken by STEM at 200

http://dx.doi.org/10.5772/61808

kV with a high-angle annular dark field (HAADF) detector. Figures 5b and 5c show the 3 and 28 layers of graphene edges corresponding to the two arrows pointed area in Fig. 5a [66]. Figure 5d displays AFM images of chemically synthesized RGO nanosheets with ~0.6 nm thickness and with lateral dimensions in a few hundred nanometers to one micrometer [67]. And Figs. 5e and 5f show the AFM images of self-assembled RGO nanosheets with a 0.9 nm thickness [71].

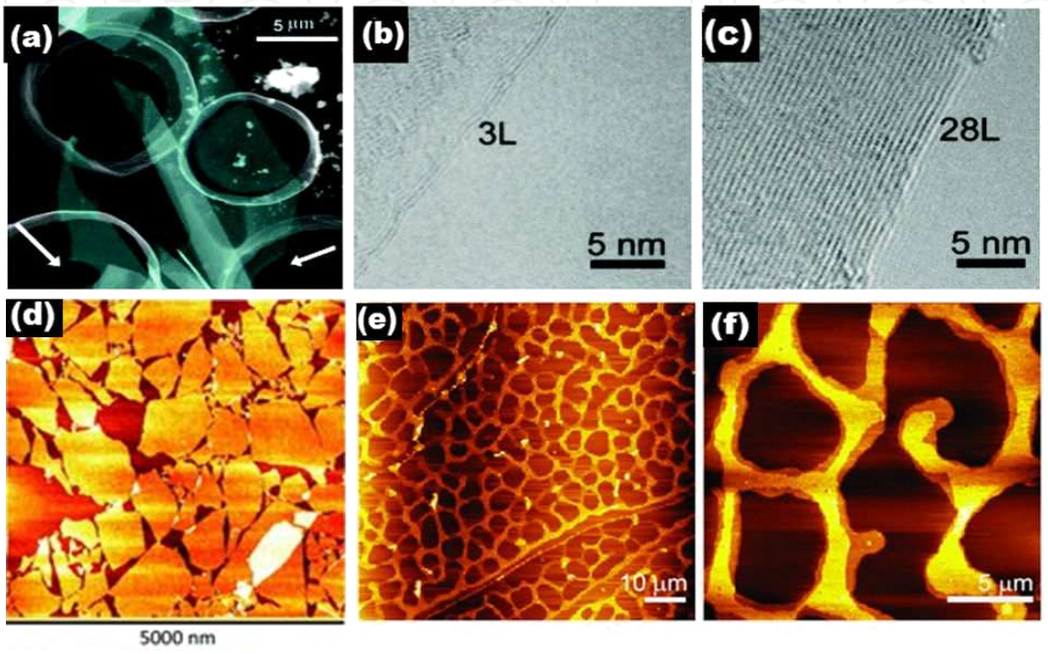

Figure 5. (a) HAADF-STEM image showing an overview of graphene flakes supported by a holey Formvar film covered with Cu grids. The arrows indicate areas where graphene is freely suspended on the holey film. (b) High-resolution TEM images of a three-layered graphene edge. (c) High-resolution TEM images of a 28-layered graphene sheet edge. (d) An AFM image of RGO nanosheet. (e,f) AFM images as an example of the self-assembled patterns of RGO nanosheets forming a bilayer nanofilm on mica surfaces. Scanned areas of AFM images are 80 μm × 80 μm (c) and 20 μm × 20 μm. (Combiningly reproduced with permission from ref. 66 Copyright Elsevier 2010, ref. 67 copyright 2013 WILEY-VCH Verlag GmbH & Co. KGaA, Weinheim, and ref. 71 copyright 2012 WILEY-VCH Verlag GmbH & Co. KGaA, Weinheim)

Figure 6 shows the morphology and structure of the 3D graphene/Co_3O_4 nanowire nanohybrid materials by SEM and TEM imaging. Figure 6a shows the SEM images of 3D porous structured graphene. Figure 6b-6d shows the uniform coverage of Co_3O_4 nanowire on 3D graphene skeleton. The high-resolution SEM image shows that the diameter of Co_3O_4 nanowire on 3D graphene is around 200–300 nm and the length is around several micrometers (Fig. 6d). And the TEM image (Fig. 6e) shows that the Co_3O_4 nanowires are composed of numerous nanoparticles.

3.2. Spectroscopic characterization

FTIR spectroscopy has been widely used to characterize different functional groups with specific chemical bonds (such as hydroxyl, carbonyl, carboxylic, and epoxy), which absorb

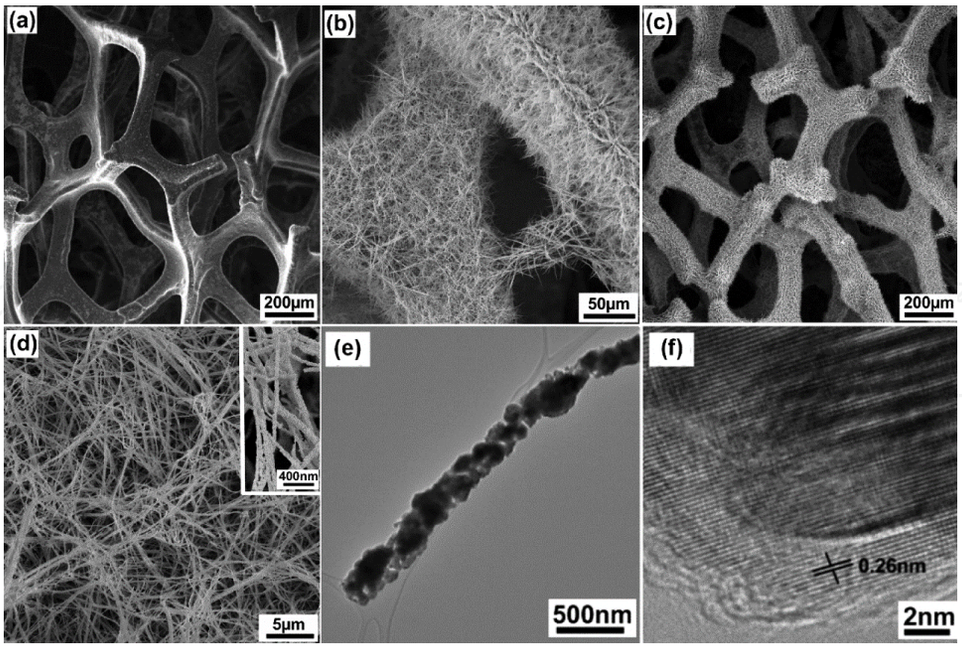

Figure 6. SEM images of (a) 3D graphene structure, (b) 3D graphene/Co_3O_4 nanowire nanohybrid (c, d) Low- and high-magnification SEM images of 3D graphene/Co_3O_4 nanowire nanohybrid material. Inset panel d shows an enlarged image. (e, f) Low- and high-resolution TEM images of Co_3O_4 nanowire grown on the 3D graphene surface. (Reproduced with permission from ref. 17 Copyright © 2012 American Chemical Society)

light energy (4000 cm^{-1} to 400 cm^{-1}) and exhibit a frequency corresponding to the fundamental vibrations [72]. Raman spectroscopy deals with the frequencies of Raman-scattered monochromatic light. As a supplementary to FTIR, Raman spectroscopy can provide sufficient information for characterization of graphene-based materials. Vibrations of different groups in polar/nonpolar molecules can be efficiently detected by these two methods. From the Raman spectra of graphene, three typical peaks of the G band at around 1580 cm^{-1}, the D band at around 1350 cm^{-1}, and the 2D band at 2700 cm^{-1} are often observed. The G band is an indicator of the stacking structures; the D is generally associated with the order/disorder of the material; the 2D-band is sensitive to the layer number of graphene sheets [2]. The ratio of the intensity of the two bands (D/G) is used for determining the number of layers in a particular graphene sample and its overall stacking behavior [2]. From Fig. 7a [16], two prominent peaks for the D and G bands are observed in the range of 1000–2000 cm^{-1}. And the intensity ratio of the D and G band indicates the density of structural defects on the graphene surface. In Fig. 7a, the I_D/I_G ratio of CuO/GO composite is 1.03 (S3), 0.96 (S2), and 0.87 (S1), which is much higher than the calculated value of GO (0.77). These ratios clearly indicate that the CuO modification introduced additional defects into the GO structure [16].

Figure 7b displays the FT-IR spectra of GO and different metal oxide nanocomposites. GO shows some typical peaks at 3420 and 1712 cm^{-1}, respectively, for the stretching vibrations of O–H and C=O. And also the bending vibration peak at 1408 cm^{-1} for O–H, at 1223 cm^{-1} for C–OH, the stretching peak at 1052 cm^{-1} for C–O, and the vibration peak at 1633 cm^{-1} for C=C [73]. For the spectra of Mn_3O_4–GNS, the vibration peaks at 610 cm^{-1} and 491 cm^{-1} are an indi-

http://dx.doi.org/10.5772/61808

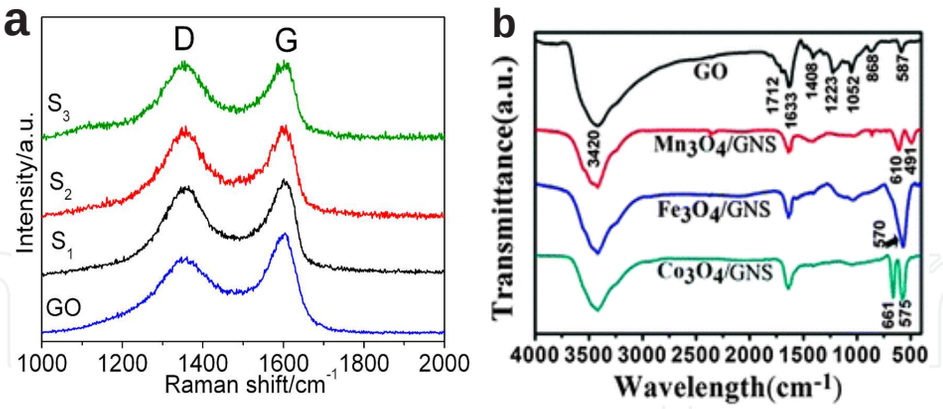

Figure 7. (a) Raman spectra of GO and CuO/GO composites and (b) FTIR spectra of GO, and Mn_3O_4–GNS, Fe_3O_4–GNS, and Co_3O_4–GNS nanocomposites. (Reproduced with permission from ref. 16. Copyright ACS 2013; from ref. 74 Copyright RSC 2012)

cation of the stretching modes of the Mn–O. In the spectrum of Fe_3O_4–GNS, the peak at 570 cm^{-1} is assigned to the vibration of the Fe–O bonds. In addition, for the spectrum of Co_3O_4–GNS, the peaks at 611 cm^{-1} and 575 cm^{-1} correspond to Co–O bonds [74].

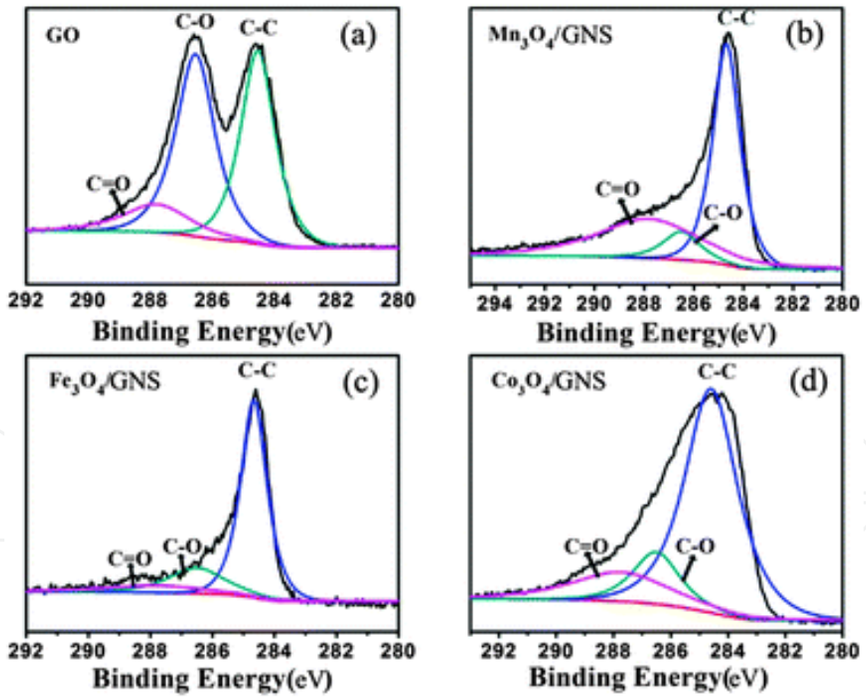

Figure 8. C 1s XPS spectra of (a) GO, (b) Mn_3O_4–GNS composite, (c) Fe_3O_4–GNS composite, and (d) Co_3O_4–GNS composite. The blue, pink, and green curves denote C–C, C–O, and C=O spectra, respectively. (Reproduced with permission from ref. 74 Copyright RSC 2012)

XPS is a powerful tool for the investigation of chemical composition, elemental states, and the nature of heteroatom functionalized or doped-graphene-based nanohybrid materials. For

example, the presence of different metal or different heteroatom on functionalized graphene can be reliably identified by XPS. Zhang et al. [74] synthesized different inorganic–organic hybrid nanocomposite materials based on reduced graphene oxide and three different metal oxides. Figure 8a shows the C 1s spectrum of GO with two strong peaks of C–C, C–O, and a relatively weak peak of C=O species. After the formation of the composites, the peaks of C–O and C=O are significantly weakened due to the removal of oxygen-containing functional groups on GO [75]. Also, by comparing Fig. 8(b)–(d), Fe_3O_4–GNS displays the lowest C–O and C=O intensity, indicating that Fe^{2+} is the most efficient ion for the reduction of GO. In addition, C 1s, O 1s, and M 2p peaks existing in the wide scan spectra of different metal nanocomposites with graphene clearly indicate the combination of graphene nanosheets and different metal oxide NPs.

Other spectroscopic techniques are also available for the characterization of nanocomposites. UV-vis spectroscopic analysis often shows some typical absorption peaks for graphene and graphene oxide at around 268, 230, and 300 nm, which is relevant to the π–π^* transitions of aromatic C=C bonds, and the n-π^* transitions of C=O bonds, respectively [76]. TGA technique has been extensively used in characterizing the thermal stability and loading amount of different metal nanoparticles in graphene-based nanocomposites [77, 79]. Energy dispersive X-ray (EDX) spectroscopy is very helpful for qualitative and quantitative analysis of the element distribution on graphene-based nanocomposite materials. EDX is more effective for determination of the locations of different metals in nanocomposites when combined with TEM or SEM [80, 81].

3.3. Main physicochemical properties

The physicochemical properties of different graphene–metal oxide nanohybrid material can be characterized by a series of electrochemical methods and instruments, such as cyclic voltammetry (CV) measurements, linear sweep voltammetry analysis (LSV), and electrochemical impedance spectroscopy (EIS). In some cases, rotating-disk electrodes (RDE) and rotating ring-disk electrodes (RRDE) are needed. Each method has its specific advantages for studying electrocatalytic performance of the hybrid materials. For the different characterizations, one method is normally not sufficient but several methods involved. In this section, we focus on discussing some electrochemical characterization techniques and their specialties and limitations.

3.3.1. Cyclic Voltammetry (CV)

CV is arguably the most common and straightforward method to determine the electrocatalytic activity of a nanocomposite material. CV is normally measured in a typical electrolyte solution at room temperature. An electrochemical cell consists of three electrodes, i.e., a working electrode loaded with the catalyst, a reference electrode, and a Pt wire as a counter electrode [82].

As shown in Fig. 9, the electrochemical kinetics of CuO/GO/GCEs compared with CuO/GCEs was studied by CV systematically. The CV was performed in 0.1 M NaOH electrolyte solution with a scan rate of 100 mV/s. Figure 9a shows a peak at +0.67 V versus Ag/AgCl from all the three CuO/GCEs electrodes, which corresponds to the Cu(II)/Cu(III) redox couple. The three

http://dx.doi.org/10.5772/61808

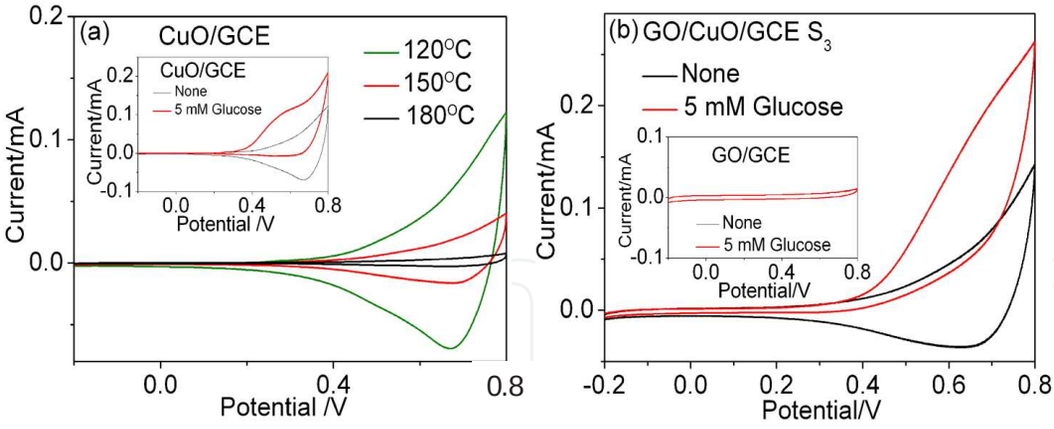

Figure 9. CV curves of (a) CuO NPs synthesized at 120, 150, and 180°C. The inset is the CuO NPs synthesized at 120°C in 0.1 M NaOH before (black trace) and after (red trace) the injection of 5 mM glucose. (b) CuO/GO composite S3 and GO sheet (inset) in 0.1 M NaOH before (black trace) and after (red trace) the injection of 5 mM glucose. (Reproduced with permission from ref. 16. Copyright ACS 2013)

different types of CuO NP generated different peak currents. CuO NPs obtained at 120°C displayed the most efficient electron transfer. The inset in Fig. 9a represents the CVs of before and after the addition of 5 mM glucose to the electrolye solutions for CuO/GCE based on 120°C CuO NPs. The Cu (II)/Cu(III) redox couple is the important factor for nonenzymatic glucose detection. Figure 9b shows the CV response of the CuO/GO/GCE before and after the addition of 5 mM glucose to the electrolye solutions, and the inset shows the CV curve of the GO/GCE electrode as a reference. As GO is electroinactive, there is no electrocatalytic oxidation of glucose. In contrast, CuO/GO/GCE showed high electrocatalytic activity, and the peak current significantly increases. Thus, the cyclic voltammetry offers a convenient way to study the electrocatalytic oxidation process of glucose.

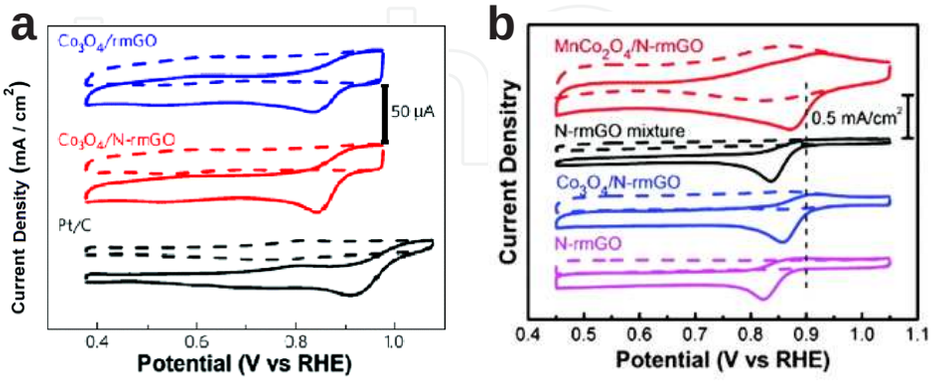

Figure 10. (a) CVs of ORR on different electrodes in N_2- and O_2-saturated 0.1 M KOH with a scan rate of 10 mV s^{-1}. (b) CV curves of $MnCo_2O_4$/N-rmGO, $MnCo_2O_4$ + N-rmGO mixture, Co_3O_4/N-rmGO, and N-rmGO on GCEs in O_2-saturated (solid line) or N_2-saturated (dash line) 1 M KOH. The peak position of Pt/C is displayed as a dashed line for comparison. (Reproduced with permission from ref. 19 Copyright Nature 2011; from ref. 18 Copyright ACS 2012)

As shown in Fig. 10a, the commercial Pt/C displays typical CV responses of ORR in N_2 and O_2-saturated 0.1 M KOH. The black dash line shows CV response in the N_2-saturated 0.1 M KOH within a potential window from 0.36 to 1.1 V. It is clearly seen that there is no sign of the typical ORR peak of Pt/C at +0.9 V [19]. However, a distinct performance of ORR (black solid line) is clearly seen in the case of O_2-saturated 0.1 M KOH. The clear peak at ~0.9 V of Pt/C indicates that the Pt/C exhibits excellent ORR activity with its standard onset potential (~1.0 V) and peak potential (~0.9 V). Figure 10b compares the electrocatalytic ORR performance of $MnCo_2O_4$/N-rmGO, N-rmGO mixture, Co_3O_4/N-rmGO, and N-rmGO in an N_2- and O_2-saturated 0.1 M KOH solution, respectively. However, these four electrodes showed different ORR activity in O_2 saturated electrolyte solutions. The ORR activity of $MnCo_2O_4$/N-rmGO (red solid line) has a more positive peak potential and higher peak current density (0.88 V, 0.5 mA cm^{-2}) than those of the N-rmGO mixture (~0.84 V, 0.38 mA cm^{-2}), Co_3O_4/N-rmGO (~0.86 V, 0.44 mA cm^{-2}), and N-rmGO (~0.82 V, 0.29 mA cm^{-2}). Therefore, $MnCo_2O_4$/N-rmGO material is more promising for ORR application, with a similar performance to that obtained at commercially available Pt/C [18].

3.3.2. Linear Sweep Voltammetry analysis (LSV)

LSV analysis is a vital method for evaluating the ORR activity of synthesized nanocomposites combining a rotating-disk electrode (RDE) or rotating ring-disk electrode (RRDE) [83, 86]. Similar to CV, the LSV analysis is also done in an O_2-saturated 0.1 M KOH electrolyte solution at different rotation rates of electrode under room temperature. For LSV, the electrolytic bath contains three electrodes: an RDE or RRDE quantitatively coated with the synthesized catalyst, an Ag|AgCl/KCl (saturated) reference electrode, and a Pt wire as an auxiliary electrode. During electrochemical measurement, the working electrode steadily rotates at the required rotation rate, and the current density changes in the potential range corresponding to the CV for one linear sweep are recorded. LSV technique has been extensively used in studying the electrocatalytic ORR kinetics and mechanism.

3.3.3. Amperometric technique (I-t)

Amperometric technique is very crucial for electrocatalytic sensing applications. For amperometric sensors, current is produced proportional to the concentration of the analyte to be detected.

Figure 11a compares the I–t curves of CuO/GCE and three CuO/GO/GCEs (S1–S3) electrode sensing glucose. Figures 11a and 11b show that the sensors produced an excellent amperometric current with a short response time. Figures 11c and 11d show the amperometric responses of CuO/GO/GCEs S3 sensor toward the electrocatalytic oxidation of glucose in human serum and the corresponding calibration curve [16]. The sensitivity, lower detection limit, and linear range can thus be calculated from these amperometric data.

3.3.4. Electrochemical Impedance Spectroscopy (EIS)

Electrochemical impedance spectroscopy (EIS) has become a popular and effective technique in recent decades for the determination of double-layer capacitance, characterization of

http://dx.doi.org/10.5772/61808

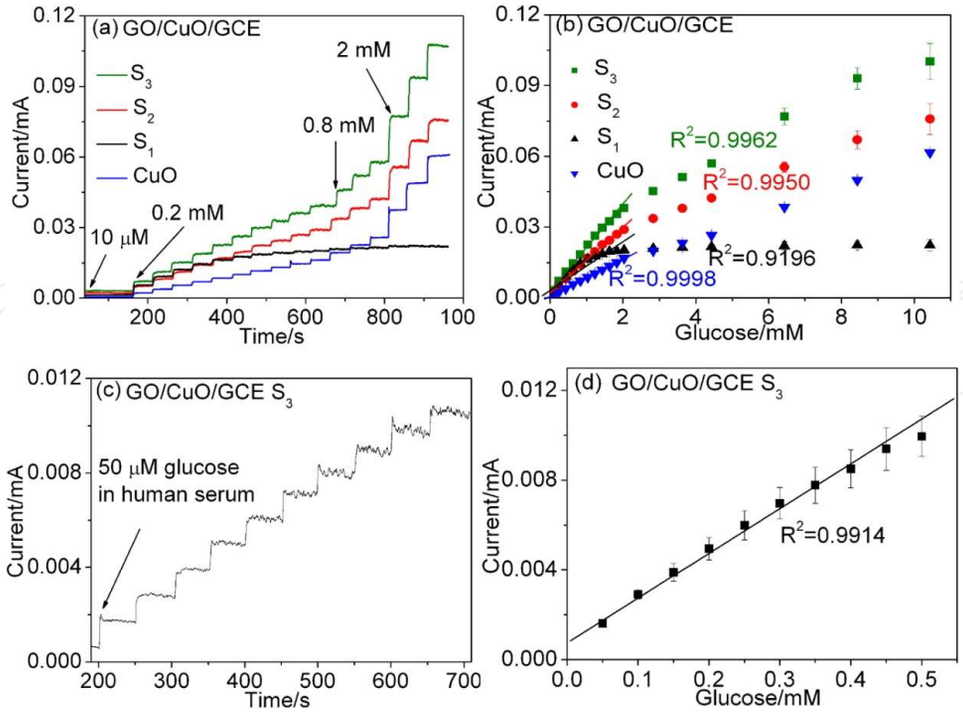

Figure 11. Amperometric responses: (a) CuO (120 °C) and three different RGO-CuO (S1, S2, and S3); (b) the corresponding calibration curves of (a); (c) S3 to successive additions of human serum contained 50 μM glucose; (d) corresponding calibration curve of (c). (Reproduced with permission from ref. 16. Copyright ACS 2013)

electrode processes, and identification of complex interfaces. EIS records the response from an electrochemical system by the stimulation of an imposed periodic small amplitude AC signal. EIS measurements are normally done at various AC frequencies, and then, the EIS can be measured by the changes of the ratio between the AC potential and current signal with the corresponding sinusoid frequencies (ω). EIS analysis has extensively been performed for ORR to explore the kinetic process of the reaction with some essential information, including the interface and structure of the ORR electrode materials, properties of electric double layer, and diffusion of oxygen. The kinetic electron transfer process for ORR is explained by an EIS plot with a semicircle and a linear portion corresponding to a charge transfer and mass transportation procedure at the high-frequency region and the low-frequency region, respectively.

4. Applications of graphene–metal oxide nanohybrids as electrocatalysts

Graphene–metal-oxide-based nanohybrid materials have a wide range of applications from electrochemical sensing to the ORR electrocatalysis, due to their superior properties and low cost [87, 88]. The new types of materials could open up a new window for superior electrocatalytic activity as well as selectivity and durability, which can act as promising electrode materials for various electrochemical reactions [89, 90, 91]. In this section, we present some examples for the applications of graphene–metal oxide nanohybrids for different kinds of electrocatalytic reactions.

4.1. Metal-oxide-decorated 2D graphene structures and electrocatalysis

If metal oxide nanoparticles are randomly loaded on graphene sheets but with little control in size and structure [92], then it can result in make the poor interaction between nanoparticles and graphene sheet [93]. Recently, the methods have been continuously improved, to some degree with controlling their locations and amount. In this context, a number of metal oxides are synthesized and loaded onto graphene matrix used as nonenzymatic sensor materials [16, 29, 31, 35, 45, 94, 95]. For example, Sun and coworkers [96] made a presynthesized monodisperse Co/CoO core/shell nanoparticles on the graphene surface (Fig. 12). In Co/CoO core/shell nanoparticles, Co core size and thickness can be tuned by controlling the oxidation conditions. In their work, they demonstrated the significance of Co/CoO size and graphene support for the tuning of electrocatalysts for efficient ORR with a selective 4e process (Fig. 12b,c).

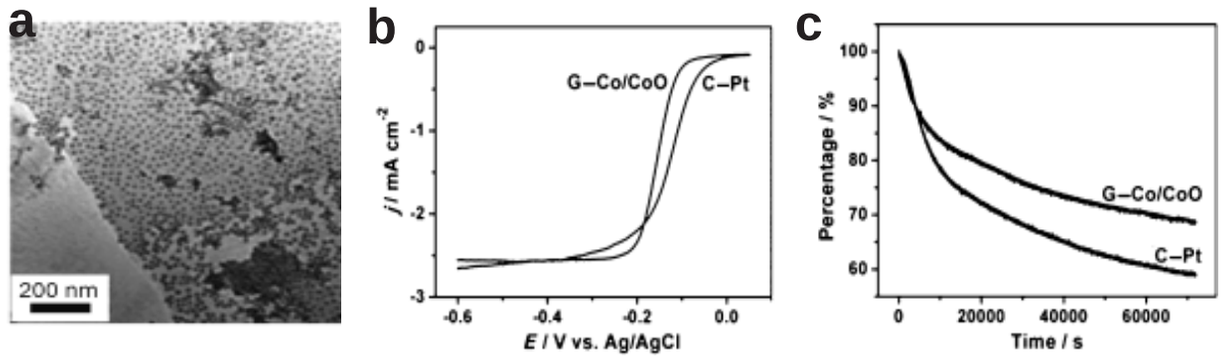

Figure 12. (a) A TEM image of the Co/CoO core/shell NPs deposited on graphene surface. (b) ORR polarization curves of the G–Co/CoO NPs and commercial C–Pt catalyst. Scan rate: 10 mV s^{-1} and rotation rate 400 rpm. (c) The chronoamperometric responses for the ORR on the G–Co/CoO NPs and commercial C–Pt catalyst at −0.3 V. Rotation rate: 200 rpm. The measurements were performed in O_2-saturated KOH (0.1 M) solution. (Reproduced with permission from ref. 96 Copyright 2012 WILEY-VCH Verlag GmbH & Co. KGaA, Weinheim)

The optimized Co/CoO–graphene electrocatalyst exhibited reasonably high activity and better stability than the commercial Pt/C catalyst. It is also evident that the ORR activity of cobalt oxide–graphene hybrid electrocatalysts is significantly enhanced with the Co content and its coupling with N-doped graphene [97]. Cobalt oxides/graphene nanohybrid materials can also serve as the ORR catalysts used in Li–O_2 batteries. Graphene sheets with Co_3O_4 nanofiber immobilized on both sides can act as a bifunctional catalyst for the ORR[98]. This excellent electrochemical performance relies on the facile electron transport and fast O_2 diffusion between the porous Co_3O_4 nanofiber networks and the ultrathin graphene layer. Manganese-oxides-based graphene nanocomposites have also been used as a stable and low-cost cathode electrocatalysts for fuel cells and Li–air batteries [99, 101]. It is clearly evident that electrocatalytic performance of metal oxide–graphene nanocomposites is closely associated with morphology and size of metal oxide nanoparticles and metal oxide–graphene electronic couplings [102]. Qiao and coworkers showed a mesoporous structure of Mn_3O_4/graphene hybrid nanomaterials with good ORR activity, excellent stability, and high selectivity [103]. Kim and coworkers also showed the ORR mechanism of a system with a lower loading (19.2%)

of Mn_3O_4 nanoparticles on graphene sheets is comparable to that of the Pt/C electrode with a 4e transfer, whereas the composite with a higher Mn_3O_4 content (52.5%) undergoes a conventional 2e process [104]. Also, other graphene-supported metal oxides, e.g., Fe_3O_4 [105], Fe_2O_3 [106], Cu_2O [107, 108], and Ru_2O [109] were also studied as electrocatalysts for ORR in fuel cells and Li–air batteries.

4.2. Metal-oxide-decorated 3D graphene structures and electrocatalysis

3D structured graphene (e.g., graphene foam) is an ideal candidate for noble metal oxide catalyst support for electrocatalytic applications because of its high electron conductivity, large surface area, sufficient porosity, and thermal stability [110]. 3D graphene can offer high surface areas for higher loading of metal oxide nanoparticles, which can show enhanced electrocatalytic activity. For example, Dong and coworkers [17] synthesized a 3D graphene–cobalt oxide nanohybrid material for high-performance supercapacitor and enzymeless glucose detection. Figure 13 shows the electrocatalytic oxidation of glucose in low-concentration alkaline solutions. Figure 13a shows the CV curves of the 3D graphene/cobalt oxide composite electrode obtained at different scan rates. Two pairs of redox peaks (I/ II and III/ IV) are observed from the CV. The redox peak currents increase with increasing scan rate proportionally, which implies a surface-controlled electrochemical process. Figure 13b shows that the oxidation current at peak III (at ~0.58 V) started increasing with introduction of glucose, but the other peak remained almost constant. Figure 13c shows the amperometric responses of the graphene/Co_3O_4 composite electrode to glucose with various concentrations. The calibration curve of the amperometric response was plotted in Fig. 13d. This composite material showed an excellent sensitivity of 3.39 mA mM^{-1} cm^{-2}, a relatively narrow linear range (up to 80 μM) and sub-100 nM lower detection limit (LOD).

Feng and Mullen have studied the controllable structural assembly of Fe_3O_4 nanoparticles on 3D N-doped graphene aerogel support [21]. Figure 14 (a-d) shows interconnected macroporous graphene hybrid network uniformly decorated with Fe_3O_4 nanoparticles. The Fe_3O_4/N–graphene aerogel network displayed excellent electrocatalytic activity for the ORR in alkaline electrolytes with a high current density, low ring current and H_2O_2 yield, being a four electron transfer number, and high stability (Fig. 14e,f). The electrocatalytic ORR has an onset potential of +0.16 V (vs Ag/AgCl) and a high current density of 1.46 mA cm^{-2}, which is well-comparable with the performance by commercial Pt/C.

4.3. Heteroatom doped-graphene-materials and their electrocatalysis

Nitrogen and sulfur are the mostly used elements for doping graphene[111, 114]. Specific doping on graphene could lead to remarkable increase in charge carrier concentration, specific surface area, and enhanced capacitance retention. The N- or S-doped graphene materials show new exciting properties compared to pristine graphene. For instance, the spin density and charge distribution of carbon atoms are modulated by the neighboring nitrogen dopants, which induce the "activation region" on the graphene surface. This kind of activated region can directly participate in electrocatalytic reactions such as ORR [115, 116] or anchor metal nanoparticles with specific catalytic activity desired [117].

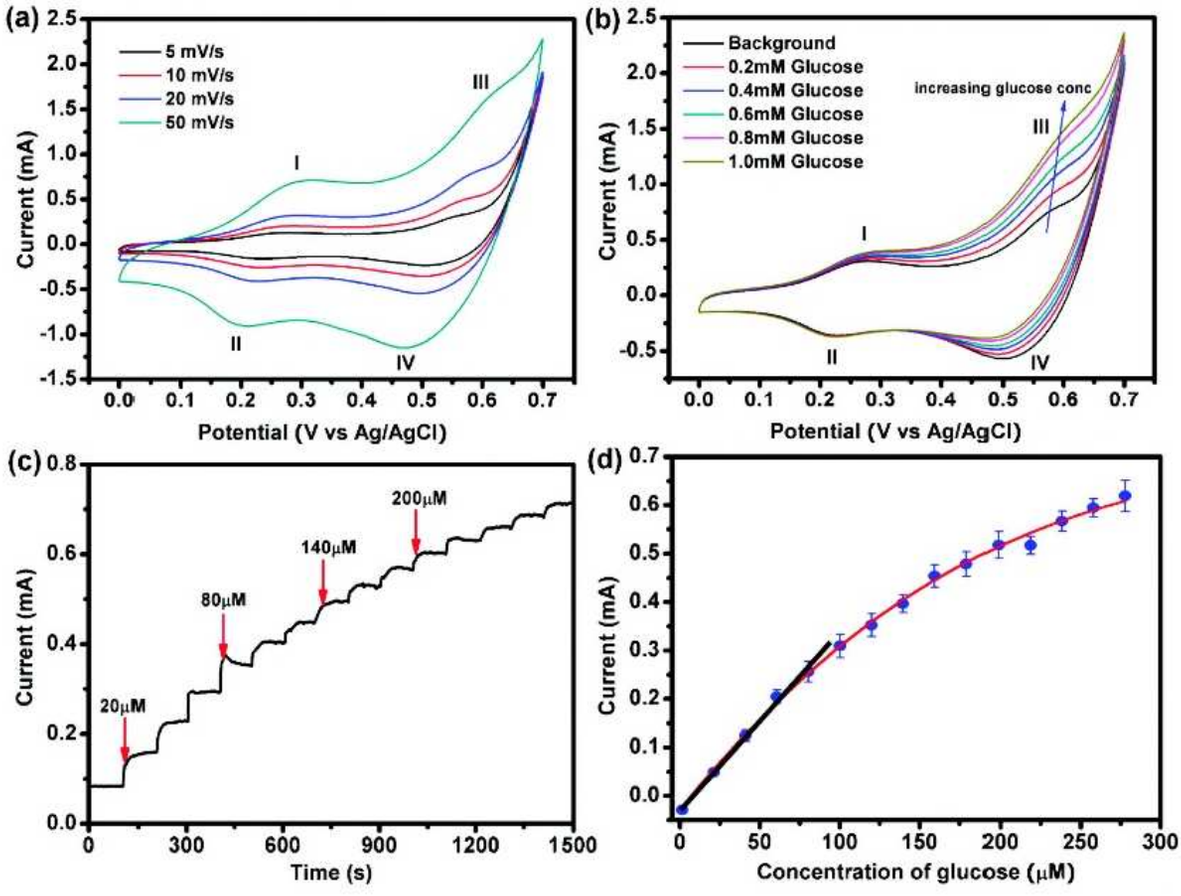

Figure 13. Electrochemical sensing of glucose in 0.1 M NaOH solution using the 3D graphene/Co_3O_4 composite electrode. (a) CV curves measured at different scan rates (5, 10, 20, and 50 mV/s). (b) CV curves in the presence of different concentrations of glucose (0, 0.2, 0.4, 0.6, 0.8, and 1 mM), at the scan rate of 20 mV/s. (c) Amperometric data of the composite electrode (potential 0.58 V) upon addition of glucose to increasing concentrations. (d) Average dose response curve (amperometric current response *vs* glucose concentration) obtained from three different sensors, with a linear fitting at lower concentration range and an exponential fitting at higher concentration range. The error bars indicate the standard deviations. (Reproduced with permission from ref. 17. Copyright ACS 2012)

Sheng et al. [118] reported a facile catalyst-free method for the synthesis of N-doped graphene via thermal annealing graphene oxide with melamine for the electrocatalytic application in ORR. Figure 15 compares cyclic voltammograms (CVs) for the electrochemical reduction of O_2 at a bare glassy carbon electrode (GCE), graphene/GCE, and NG/GCE in O_2-saturated 0.1 M KOH solutions. The onset potential of ORR at the NG/GCE occurs at 0.1 V, which is about 0.1 V more positive than that of graphene/GCE. The electrocatalytic process of NG/GCE is a one-step four-electron pathway for ORR, which is almost twice as large as that for pristine graphene in the current density. Sulfur-doped graphene was successfully prepared using GO and benzyl disulfide as precursors under high temperature, and the as-prepared temperature-dependant S-Doped graphene was tested as a metal-free cathode catalyst for oxygen reduction. All the results further confirmed that the S-doped graphene is a promising material with high catalytic activity for ORR [119]. N and S co-doped graphene was also developed and used for ORR recently; compared to the single element doped graphene, co-doped graphene displayed even more efficient electrocatalysis toward ORR [120].

http://dx.doi.org/10.5772/61808

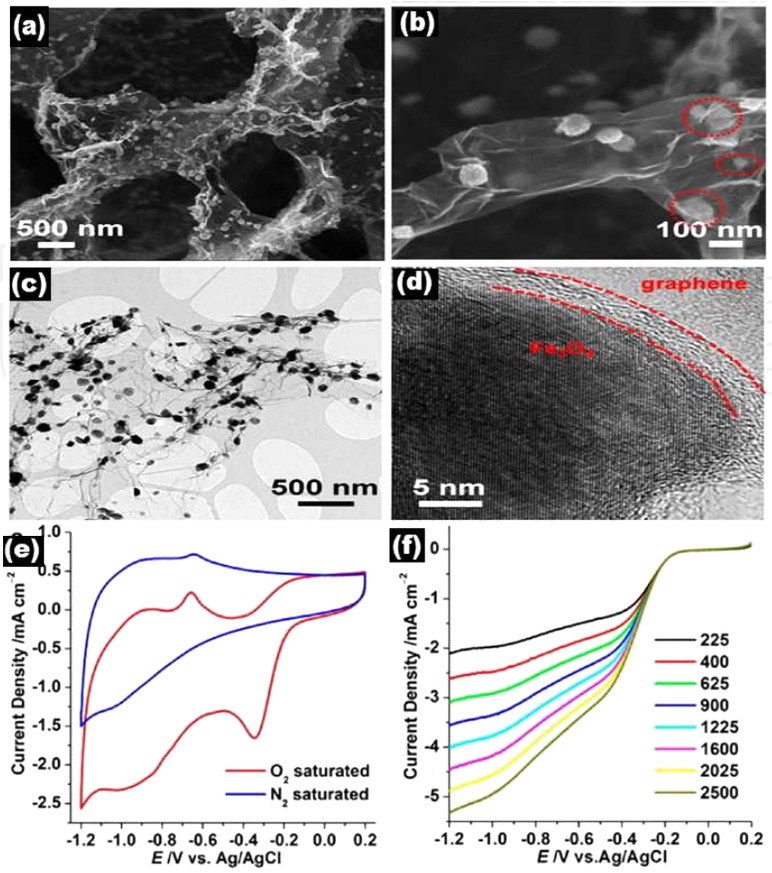

Figure 14. (a,b) Typical SEM images of Fe_3O_4/N-Gas, revealing the 3D macroporous structure and uniform distribution of Fe_3O_4 NPs in the GAs. The red rings in (d) indicate Fe_3O_4NPs encapsulated in thin graphene layers. Representative (c) TEM and (d) HRTEM images of Fe_3O_4/N-Gas, revealing an Fe_3O_4 NP wrapped by graphene layers. (e) CVs of Fe_3O_4/N-GAs in N_2- and O_2-staturated 0.1 M aqueous KOH electrolyte solution at a scan rate of 100 mV s^{-1}. (f) LSVs of Fe_3O_4/N-GAs in O_2-saturated 0.1 M KOH at a scan rate of 10 mV s^{-1} at different RDE rotation rates (in rpm). (Reproduced with permission from ref. 21. Copyright ACS 2012)

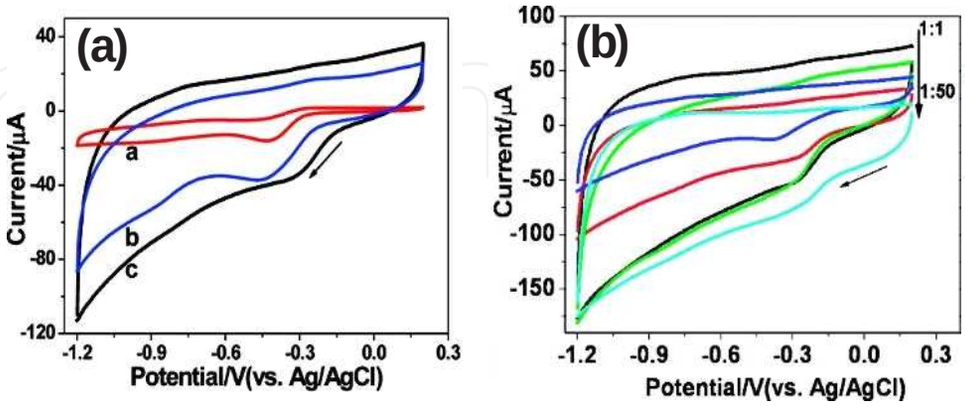

Figure 15. (a) Cyclic voltammograms (CVs) for ORR obtained at a bare GCE (a), graphene/GCE (b), and NG5/GCE (N % = 7.1%) (c) in O_2-saturated 0.1 M KOH aqueous solution. (B) CVs for ORR at NGs, synthesized with different mass ratio of GO and melamine (1:1, 1:2, 1:5, 1:10, 1:50) at 800°C, modified GCE in O_2-saturated 0.1 M KOH aqueous solution. Scan rate: 100 mV/s. (Reproduced with permission from ref. 118 Copyright ACS 2011)

5. Conclusions and outlook

The rapid development of graphene-based nanohybrid electrocatalysts for energy conversion, storage, and various electrochemical sensors has been driven by their unique structural features, novel physicochemical properties, high stability, and low cost. The immobilization of transition metal oxides on graphene by various methods via the use of interactions between the structural defects and functional groups on graphene's surface, contributed to the improved catalytic activity and stability of graphene-based transition metal oxide nanohybrid catalysts. In this chapter, we have discussed the recent development of graphene-supported transition metal oxide nanohybrid materials for their sensor and energy applications, including their synthesis, structural characterizations, key properties, and major applications. The control in the morphology and dimension of the graphene-based nanocomposite is of crucial importance for their electrocatalytic activities. As a consequence, multivalent transition metal oxides with special structural properties exhibit more efficiency for the electrocatalytic reactions than amorphous nanocomposites under similar experimental conditions. Electrocatalytic performance of graphene-based transition metal nanohybrid materials can be characterized by different electrochemical techniques in detail. Stability and durability are among the most important factors for promising electrocatalytic applications. The flexibility and large surface area of graphene sheets could prevent particles from agglomerationand facilitate accommodation of large amount of particles. Monotransition metal oxides anchored on graphene have already shown good electrocatalytic performance with long-term stability. However, the strategy of synthesizing bimetallic transition metal oxides is very promising for further elevating the electrocatalytic activity. Also, covalently bonded bimetallic oxides on graphene can offer better activity and longer durability than the physical mixture of two types of metallic nanoparticles. Therefore, the rational design of cationic substitution and covalent coupling with graphene supports can instruct the construction of advanced electrocatalysts for sensor- and energy-related applications. Thus, the advancement of sophisticated structure-controlled methods and processes for the *in situ* synthesis of graphene-based transition metal oxide nanocomposites is crucial for the development of next-generation electrocatalysts. It should be noted, however, that the fundamental mechanisms behind the electrocatalytic performance of graphene-based nanocomposites are far from being fully understood. Moreover, the electronic interactions between graphene and nanoparticles and the synergistic effects are needed to be explored. These remained challenges will motivate strongly many ongoing research and further development of this field.

Author details

Arnab Halder, Minwei Zhang and Qijin Chi*

*Address all correspondence to: cq@kemi.dtu.dk

Department of Chemistry, Technical University of Denmark, Kongens Lyngby, Denmark

References

[1] A.K. Geim and K.S. Novoselov, "The Rise of Graphene," *Nat. Mater.*, vol. 6, no. 3, pp. 183–191, Mar. 2007.

[2] D. R. Dreyer, S. Park, C. W. Bielawski, and R. S. Ruoff, "The Chemistry of Graphene Oxide," *Chem. Soc. Rev.*, vol. 39, no. 1, pp. 228–40, Jan. 2010.

[3] Y. Zhu, S. Murali, W. Cai, X. Li, J. W. Suk, J. R. Potts, and R. S. Ruoff, "Graphene and Graphene Oxide: Synthesis, Properties, and Applications," *Adv. Mater.*, vol. 22, no. 35, pp. 3906–3924, 2010.

[4] X. Huang, Z. Yin, S. Wu, X. Qi, Q. He, Q. Zhang, Q. Yan, F. Boey, and H. Zhang, "Graphene-Based Materials: Synthesis, Characterization, Properties, and Applications," *Small*, vol. 7, no. 14, pp. 1876–1902, 2011.

[5] C. Lee, X. Wei, J. W. Kysar, and J. Hone, "Measurement of the Elastic Properties and Intrinsic Strength of Monolayer Graphene," *Science*, vol. 321, no. 5887, pp. 385–388, Jul. 2008.

[6] A. A. Balandin, S. Ghosh, W. Bao, I. Calizo, D. Teweldebrhan, F. Miao, and C. N. Lau, "Superior Thermal Conductivity of Single-Layer Graphene," *Nano Lett.*, vol. 8, no. 3, pp. 902–907, Mar. 2008.

[7] J. A. Farmer and C. T. Campbell, "Ceria Maintains Smaller Metal Catalyst Particles by Strong Metal-Support Bonding," *Science*, vol. 329, no. 5994, pp. 933–936, Aug. 2010.

[8] R. S. Dey, H. A. Hjuler, and Q. Chi, "Approaching the Theoretical Capacitance of Graphene through Copper Foam Integrated Three-Dimensional Graphene Networks," *J. Mater. Chem. A*, vol. 3, no. 12, pp. 6324–6329, 2015.

[9] R. S. Dey and C. R. Raj, "Development of an Amperometric Cholesterol Biosensor Based on Graphene-Pt Nanoparticle Hybrid Material," *J. Phys. Chem. C*, vol. 114, no. 49, pp. 21427–21433, 2010.

[10] S. Giri, D. Ghosh, and C. K. Das, "Growth of Vertically Aligned Tunable Polyaniline on Graphene/ZrO 2 Nanocomposites for Supercapacitor Energy-Storage Application," *Adv. Funct. Mater.*, pp. 1312–1324, Oct. 2013.

[11] B. Anasori, M. Beidaghi, and Y. Gogotsi, "Graphene - Transition metal oxide hybrid materials," *Mater. Today*, vol. 17, no. 5, pp. 253–254, 2014.

[12] S. Gan, L. Zhong, C. Engelbrekt, J. Zhang, D. Han, J. Ulstrup, Q. Chi, and L. Niu, "Graphene Controlled H- and J-Stacking of Perylene Dyes into Highly Stable Supramolecular Nanostructures for Enhanced Photocurrent Generation," *Nanoscale*, vol. 6, no. 18, p. 10516 - 10523, 2014.

[13] W. Il Park, C.-H. Lee, J. M. Lee, N.-J. Kim, and G.-C. Yi, "Inorganic Nanostructures Grown on Graphene Layers," *Nanoscale*, vol. 3, no. 9, pp. 3522–3533, 2011.

[14] Y. Wang, L. Cheng, F. Li, H. Xiong, and Y. Xia, "High Electrocatalytic Performance of Mn_3O_4/Mesoporous Carbon Composite for Oxygen Reduction in Alkaline Solutions," *Chem. Mater.*, vol. 19, no. 8, pp. 2095–2101, 2007.

[15] F. Cheng, Y. Su, J. Liang, Z. Tao, and J. Chen, "MnO_2-Based Nanostructures as Catalysts for Electrochemical Oxygen Reduction in Alkaline Media," *Chem. Mater.*, vol. 22, no. 3, pp. 898–905, 2010.

[16] J. Song, L. Xu, C. Zhou, R. Xing, Q. Dai, D. Liu, and H. Song, "Synthesis of Graphene Oxide Based CuO Nanoparticles Composite Electrode for Highly Enhanced Nonenzymatic Glucose Detection," *ACS Appl. Mater. Interf.*, vol. 5, no. 24, pp. 12928–12934, Dec. 2013.

[17] X.-C. Dong, H. Xu, X.-W. Wang, Y.-X. Huang, M. B. Chan-Park, H. Zhang, L.-H. Wang, W. Huang, and P. Chen, "3D Graphene-Cobalt Oxide Electrode for High-Performance Supercapacitor and Enzymeless Glucose Detection," *ACS Nano*, vol. 6, no. 4, pp. 3206–3213, Apr. 2012.

[18] Y. Liang, H. Wang, J. Zhou, Y. Li, J. Wang, T. Regier, and H. Dai, "Covalent Hybrid of Spinel Manganese-Cobalt Oxide and Graphene as Advanced Oxygen Reduction Electrocatalysts," *J. Am. Chem. Soc.*, vol. 134, no. 7, pp. 3517–3523, 2012.

[19] Y. Liang, Y. Li, H. Wang, J. Zhou, J. Wang, T. Regier, and H. Dai, "Co_3O_4 Nanocrystals on Graphene as a Synergistic Catalyst for Oxygen Reduction Reaction," *Nat. Mater.*, vol. 10, no. 10, pp. 780–786, 2011.

[20] M. Wang, J. Huang, M. Wang, D. Zhang, and J. Chen, "Electrochemical Nonenzymatic Sensor Based on CoO Decorated Reduced Graphene Oxide for the Simultaneous Determination of Carbofuran and Carbaryl in Fruits and Vegetables," *Food Chem.*, vol. 151, pp. 191–197, 2014.

[21] Z.-S. Wu, S. Yang, Y. Sun, K. Parvez, X. Feng, and K. Müllen, "3D Nitrogen-Doped Graphene Aerogel-Supported Fe_3O_4 Nanoparticles as Efficient Electrocatalysts for the Oxygen Reduction Reaction," *J. Am. Chem. Soc.*, vol. 134, no. 22, pp. 9082–9085, Jun. 2012.

[22] Y. Zhou, Q. Bao, L. A. L. Tang, Y. Zhong, and K. P. Loh, "Hydrothermal Dehydration for the 'Green' Reduction of Exfoliated Graphene Oxide to Graphene and Demonstration of Tunable Optical Limiting Properties," *Chem. Mater.*, vol. 21, no. 13, pp. 2950–2956, Jul. 2009.

[23] R. Zhou, Y. Zheng, D. Hulicova-Jurcakova, and S. Z. Qiao, "Enhanced Electrochemical Catalytic Activity by Copper Oxide Grown on Nitrogen-Doped Reduced Graphene Oxide," *J. Mater. Chem. A*, vol. 1, no. 42, p. 13179 - 13184, 2013.

[24] X.-Y. Yan, X.-L. Tong, Y.-F. Zhang, X.-D. Han, Y.-Y. Wang, G.-Q. Jin, Y. Qin, and X.-Y. Guo, "Cuprous Oxide Nanoparticles Dispersed on Reduced Graphene Oxide as an

Efficient Electrocatalyst for Oxygen Reduction Reaction," *Chem. Commun.*, vol. 48, no. 13, p. 1892 - 1895, 2012.

[25] X. Liu, H. Zhu, and X. Yang, "An Amperometric Hydrogen Peroxide Chemical Sensor Based on Graphene-Fe $_3$O $_4$ Multilayer Films Modified ITO Electrode," *Talanta*, vol. 87, no. 1, pp. 243–248, 2011.

[26] H. Teymourian, A. Salimi, and S. Khezrian, "Fe_3O_4 Magnetic Nanoparticles/Reduced Graphene Oxide Nanosheets as a Novel Electrochemical and Bioeletrochemical Sensing Platform," *Biosens. Bioelectron.*, vol. 49, pp. 1–8, Nov. 2013.

[27] L. Li, Z. Du, S. Liu, Q. Hao, Y. Wang, Q. Li, and T. Wang, "A Novel Nonenzymatic Hydrogen Peroxide Sensor Based on MnO_2/Graphene Oxide Nanocomposite," *Talanta*, vol. 82, no. 5, pp. 1637–1641, 2010.

[28] X. Zhu, Y. Zhu, S. Murali, M. D. Stoller, and R. S. Ruoff, "Reduced Graphene Oxide/Tin Oxide Composite as an Enhanced Anode Material for Lithium Ion Batteries Prepared by Homogenous Coprecipitation," *J. Power Sources*, vol. 196, no. 15, pp. 6473–6477, 2011.

[29] Y. Tian, Y. Liu, W. Wang, X. Zhang, and W. Peng, "CuO Nanoparticles on Sulfur-Doped Graphene for Nonenzymatic Glucose Sensing," *Electrochim. Acta*, vol. 156, pp. 244–251, 2015.

[30] X. Zhu, Y. Zhu, S. Murali, M. D. Stoller, and R. S. Ruoff, "Nanostructured Reduced Graphene Oxide/Fe_2O_3 Composite as a High-Performance Anode Material for Lithium Ion Batteries," *ACS Nano*, vol. 5, no. 4, pp. 3333–3338, 2011.

[31] Z. Luo, X. Ma, D. Yang, L. Yuwen, X. Zhu, L. Weng, and L. Wang, "Synthesis of Highly Dispersed Titanium Dioxide Nanoclusters on Reduced Graphene Oxide for Increased Glucose Sensing," *Carbon*, vol. 57, pp. 470–476, 2013.

[32] H.-L. Guo, X.-F. Wang, Q.-Y. Qian, F.-B. Wang, and X.-H. Xia, "A Green Approach to the Synthesis of Graphene Nanosheets," *ACS Nano*, vol. 3, no. 9, pp. 2653–2659, Sep. 2009.

[33] D. Ye, G. Liang, H. Li, J. Luo, S. Zhang, H. Chen, and J. Kong, "A Novel Nonenzymatic Sensor Based on CuO Nanoneedle/Graphene/Carbon Nanofiber Modified Electrode for Probing Glucose in Saliva," *Talanta*, vol. 116, pp. 223–230, 2013.

[34] F. Xiao, Y. Li, X. Zan, K. Liao, R. Xu, and H. Duan, "Growth of Metal-Metal Oxide Nanostructures on Freestanding Graphene Paper for Flexible Biosensors," *Adv. Funct. Mater.*, vol. 22, no. 12, pp. 2487–2494, Jun. 2012.

[35] D. L. Zhou, J. J. Feng, L. Y. Cai, Q. X. Fang, J. R. Chen, and A. J. Wang, "Facile Synthesis of Monodisperse Porous Cu_2O Nanospheres on Reduced Graphene Oxide for Non-Enzymatic Amperometric Glucose Sensing," *Electrochim. Acta*, vol. 115, pp. 103–108, 2014.

[36] X. Zhang, Q. Liao, S. Liu, W. Xu, Y. Liu, and Y. Zhang, "CuNiO Nanoparticles Assembled on Graphene as an Effective Platform for Enzyme-Free Glucose Sensing," *Anal. Chim. Acta*, vol. 858, pp. 49–54, 2015.

[37] F. Xu, M. Deng, G. Li, S. Chen, and L. Wang, "Electrochemical Behavior of Cuprous Oxide-Reduced Graphene Oxide Nanocomposites and their Application in Nonenzymatic Hydrogen Peroxide Sensing," *Electrochim. Acta*, vol. 88, pp. 59–65, 2013.

[38] C. L. Sun, W. L. Cheng, T. K. Hsu, C. W. Chang, J. L. Chang, and J. M. Zen, "Ultrasensitive and Highly Stable Nonenzymatic Glucose Sensor by a CuO/Graphene-Modified Screen-Printed Carbon Electrode Integrated with Flow-Injection Analysis," *Electrochem. commun.*, vol. 30, pp. 91–94, 2013.

[39] M. Liu, R. Liu, and W. Chen, "Graphene Wrapped Cu_2O Nanocubes: Non-Enzymatic Electrochemical Sensors for the Detection of Glucose and Hydrogen Peroxide with Enhanced Stability," *Biosens. Bioelectron.*, vol. 45, pp. 206–212, Jul. 2013.

[40] S. Yang, G. Cui, S. Pang, Q. Cao, U. Kolb, X. Feng, J. Maier, and K. Müllen, "Fabrication of Cobalt and Cobalt Oxide/Graphene Composites: Towards High-Performance Anode Materials for Lithium Ion Batteries," *ChemSusChem*, vol. 3, no. 2, pp. 236–239, 2010.

[41] S. Ci, S. Mao, T. Huang, Z. Wen, D. A. Steeber, and J. Chen, "Enzymeless Glucose Detection Based on CoO/Graphene Microsphere Hybrids," *Electroanalysis*, vol. 26, no. 6, pp. 1326–1334, 2014.

[42] Y. Ye, T. Kong, X. Yu, Y. Wu, K. Zhang, and X. Wang, "Enhanced Nonenzymatic Hydrogen Peroxide Sensing with Reduced Graphene Oxide/Ferroferric Oxide Nanocomposites," *Talanta*, vol. 89, pp. 417–421, 2012.

[43] Z. Wu, S. Yang, Y. Sun, K. Parvez, and X. Feng, "3D Nitrogen-Doped Graphene Aerogel-Supported Fe_3O_4 Nanoparticles as E ffi cient Electrocatalysts for the Oxygen Reduction Reaction," *J. Am. Chem. Soc.*, vol. 134, no. 22, pp. 9082–9085, 2012.

[44] T. Gan, J. Sun, K. Huang, L. Song, and Y. Li, "A Graphene Oxide-Mesoporous MnO_2 Nanocomposite Modified Glassy Carbon Electrode as a Novel and Efficient Voltammetric Sensor for Simultaneous Determination of Hydroquinone and Catechol," *Sensors Actuators B Chem.*, vol. 177, pp. 412–418, 2013.

[45] F. Xiao, Y. Li, H. Gao, S. Ge, and H. Duan, "Growth of Coral-like PtAu-MnO_2 Binary Nanocomposites on Free-Standing Graphene Paper for Flexible Nonenzymatic Glucose Sensors," *Biosens. Bioelectron.*, vol. 41, pp. 417–423, Mar. 2013.

[46] X. Zhu, P. Zhang, S. Xu, X. Yan, and Q. Xue, "Free-Standing Three-Dimensional Graphene/Manganese Oxide Hybrids As Binder-Free Electrode Materials for Energy Storage Applications," *ACS Appl. Mater. Interfaces*, vol. 6, no. 14, pp. 11665–11674, 2014.

[47] Q. Tang, L. Jiang, J. Liu, S. Wang, and G. Sun, "Effect of Surface Manganese Valence of Manganese Oxides on the Activity of the Oxygen Reduction Reaction in Alkaline Media," *ACS Catal.*, vol. 4, no. 2, pp. 457–463, 2014.

[48] W. J. Basirun, M. Sookhakian, S. Baradaran, Z. Endut, M. R. Mahmoudian, M. Ebadi, R. Yousefi, H. Ghadimi, and S. Ahmed, "Graphene Oxide Electrocatalyst on MnO_2 Air Cathode as an Efficient Electron Pump for Enhanced Oxygen Reduction in Alkaline Solution," *Sci. Rep.*, vol. 5, p. 9108-9115, 2015.

[49] B. Yuan, C. Xu, D. Deng, Y. Xing, L. Liu, H. Pang, and D. Zhang, "Graphene Oxide/Nickel Oxide Modified Glassy Carbon Electrode for Supercapacitor and Nonenzymatic Glucose Sensor," *Electrochim. Acta*, vol. 88, pp. 708–712, 2013.

[50] Y. Zhang, Y. Wang, J. Jia, and J. Wang, "Nonenzymatic Glucose Sensor Based on Graphene Oxide and Electrospun NiO Nanofibers," *Sensors Actuators B Chem.*, vol. 171–172, pp. 580–587, Aug. 2012.

[51] X. Zhu, Q. Jiao, C. Zhang, X. Zuo, X. Xiao, Y. Liang, and J. Nan, "Amperometric Nonenzymatic Determination of Glucose Based on a Glassy Carbon Electrode Modified with Nickel(II) Oxides and Graphene," *Microchim. Acta*, vol. 180, no. 5–6, pp. 477–483, 2013.

[52] H. Zhang, J. Feng, T. Fei, S. Liu, and T. Zhang, "SnO_2 Nanoparticles-Reduced Graphene Oxide Nanocomposites for NO_2 Sensing at Low Operating Temperature," *Sensors Actuators, B Chem.*, vol. 190, no. 2, pp. 472–478, 2014.

[53] Y. Fan, K.-J. Huang, D.-J. Niu, C.-P. Yang, and Q.-S. Jing, "TiO_2-Graphene Nanocomposite for Electrochemical Sensing of Adenine and Guanine," *Electrochim. Acta*, vol. 56, no. 12, pp. 4685–4690, Apr. 2011.

[54] T. Gan, J. Sun, W. Meng, L. Song, and Y. Zhang, "Electrochemical Sensor Based on Graphene and Mesoporous TiO_2 for the Simultaneous Determination of Trace Colourants in Food," *Food Chem.*, vol. 141, no. 4, pp. 3731–3737, 2013.

[55] A. Titanium, O. Titanium, and H. C. Performance, "Synthesis of Size-Tunable Anatase TiO_2 Nanospindles and Their Assembly into Anatase@Titanium Oxynitride/Titanium Nitride–Graphene Nanocomposites for Rechargeable Lithium Ion Batteries with High Cycling Performance," *ACS Nano*, vol. 4, no. 11, pp. 6515–6526, 2010.

[56] D. Wang, D. Choi, J. Li, Z. Yang, Z. Nie, R. Kou, D. Hu, C. Wang, L. V Saraf, J. Zhang, I. a Aksay, and J. Liu, "Self-Assembled TiO_2 – Graphene Hybrid Nanostructures for Enhanced Li-Ion Insertion," *ACS Nano*, vol. 3, no. 4, pp. 907–914, 2009.

[57] K. Tiido, N. Alexeyeva, M. Couillard, C. Bock, B. R. MacDougall, and K. Tammeveski, "Graphene–TiO_2 Composite Supported Pt Electrocatalyst for Oxygen Reduction Reaction," *Electrochim. Acta*, vol. 107, pp. 509–517, Sep. 2013

[58] Z. Li, H. Zhang, Q. Liu, Y. Liu, L. Stanciu, and J. Xie, "Hierarchical Nanocomposites of Vanadium Oxide Thin Film Anchored on Graphene as High-Performance Cathodes in Li-Ion Batteries," *ACS Appl. Mater. Interfaces*, vol. 6, pp. 18894-18900, 2014

[59] Q. Liu, Z. Li, Y. Liu, H. Zhang, Y. Ren, C. Sun, W. Lu, Y. Zhou, L. Stanciu, E. a Stach, and J. Xie, "Graphene-Modified Nanostructured Vanadium Pentoxide Hybrids with Extraordinary Electrochemical Performance for Li-Ion Batteries," *Nat. Commun.*, vol. 6, pp. 1–10, 2015.

[60] G. Ye, Y. Gong, K. Keyshar, E. a. M. Husain, G. Brunetto, S. Yang, R. Vajtai, and P. M. Ajayan, "3D Reduced Graphene Oxide Coated V_2 O_5 Nanoribbon Scaffolds for High-Capacity Supercapacitor Electrodes," *Part. Part. Syst. Charact.*vol. 32, pp. 817–821, 2015.

[61] X. Dong, Y. Cao, J. Wang, M. B. Chan-Park, L. Wang, W. Huang, and P. Chen, "Hybrid Structure of Zinc Oxide Nanorods and Three Dimensional Graphene Foam for Supercapacitor and Electrochemical Sensor Applications," *RSC Adv.*, vol. 2, no. 10, pp. 4364–4369, 2012.

[62] C. Yang, L. Hu, H.-Y. Zhu, Y. Ling, J.-H. Tao, and C.-X. Xu, "rGO Quantum Dots/ZnO Hybrid Nanofibers Fabricated Using Electrospun Polymer Templates and Applications in Drug Screening Involving an Intracellular H_2O_2 Sensor," *J. Mater. Chem. B*, vol. 3, pp. 2651–2659, 2015.

[63] M. Sawangphruk, P. Srimuk, P. Chiochan, A. Krittayavathananon, S. Luanwuthi, and J. Limtrakul, "High-Performance Supercapacitor of Manganese Oxide/Reduced Graphene Oxide Nanocomposite Coated on Flexible Carbon Fiber Paper," *Carbon*, vol. 60, pp. 109–116, 2013.

[64] Y. Liu, S. Shrestha, and W. E. Mustain, "Synthesis of Nanosize Tungsten Oxide and Its Evaluation as an Electrocatalyst Support for Oxygen Reduction in Acid Media," *ACS Catal.*, vol. 2, no. 3, pp. 456–463, 2012.

[65] C. Gómez-Navarro, J. C. Meyer, R. S. Sundaram, A. Chuvilin, S. Kurasch, M. Burghard, K. Kern, and U. Kaiser, "Atomic Structure of Reduced Graphene Oxide," *Nano Lett.*, vol. 10, no. 4, pp. 1144–1148, 2010.

[66] F. Q. Song, Z. Y. Li, Z. W. Wang, L. He, M. Han, and G. H. Wang, "Free-Standing Graphene by Scanning Transmission Electron Microscopy," *Ultramicroscopy*, vol. 110, no. 12, pp. 1460–1464, 2010.

[67] N. Zhu, S. Han, S. Gan, J. Ulstrup, and Q. Chi, "Graphene Paper Doped with Chemically Compatible Prussian Blue Nanoparticles as Nanohybrid Electrocatalyst," *Adv. Funct. Mater.*, vol. 23, no. 42, pp. 5297–5306, Nov. 2013.

[68] J. C. Koepke, J. D. Wood, D. Estrada, Z.-Y. Ong, K. T. He, E. Pop, and J. W. Lyding, "Atomic-Scale Evidence for Potential Barriers and Strong Carrier Scattering at Gra-

phene Grain Boundaries: A Scanning Tunneling Microscopy Study," *ACS Nano*, vol. 7, no. 1, pp. 75–86, 2013.

[69] E. Y. Polyakova (Stolyarova), K. T. Rim, D. Eom, K. Douglass, R. L. Opila, T. F. Heinz, A. V Teplyakov, and G. W. Flynn, "Scanning Tunneling Microscopy and X-ray Photoelectron Spectroscopy Studies of Graphene Films Prepared by Sonication-Assisted Dispersion," *ACS Nano*, vol. 5, no. 8, pp. 6102–6108, 2011.

[70] G. Dong and J. W. M. Frenken, "Kinetics of Graphene Formation on Rh(111) Investigated by In Situ Scanning Tunneling Microscopy," *ACS Nano*, vol. 7, no. 8, pp. 7028–7033, 2013.

[71] S. Gan, L. Zhong, T. Wu, D. Han, J. Zhang, J. Ulstrup, Q. Chi, and L. Niu, "Spontaneous and Fast Growth of Large-Area Graphene Nanofilms Facilitated by Oil/Water Interfaces.," *Adv. Mater.*, vol. 24, no. 29, pp. 3958–64, Aug. 2012.

[72] T. Ando, M. Ishii, M. Kamo, and Y. Sato, "Thermal Hydrogenation of Diamond Surfaces Studied by Diffuse Reflectance Fourier-Transform Infrared Temperature-Programmed Desorption and Laser Raman Spectroscopy," *J. Chem. Soc. Faraday Trans.*, vol. 89, no. 11, pp. 1783–1789, 1993.

[73] Y. Xu, H. Bai, G. Lu, C. Li, and G. Shi, "Flexible Graphene Films via the Filtration of Water-Soluble Noncovalent Functionalized Graphene Sheets," *J. Am. Chem. Soc.*, vol. 130, no. 18, pp. 5856–5857, May 2008.

[74] W. Zhang, F. Liu, Q. Li, Q. Shou, J. Cheng, L. Zhang, B. J. Nelson, and X. Zhang, "Transition Metal Oxide and Graphene Nanocomposites for High-Performance Electrochemical Capacitors," *Phys. Chem. Chem. Phys.*, vol. 14, no. 47, pp. 16331–16337, 2012.

[75] Z.-J. Fan, W. Kai, J. Yan, T. Wei, L.-J. Zhi, J. Feng, Y. Ren, L.-P. Song, and F. Wei, "Facile Synthesis of Graphene Nanosheets via Fe Reduction of Exfoliated Graphite Oxide," *ACS Nano*, vol. 5, no. 1, pp. 191–198, Jan. 2011.

[76] Z. Sun, Z. Yan, J. Yao, E. Beitler, Y. Zhu, and J. M. Tour, "Growth of Graphene from Solid Carbon Sources," *Nature*, vol. 468, no. 7323, pp. 549–552, Nov. 2010.

[77] J. Shen, X. Li, N. Li, and M. Ye, "Facile Synthesis of $NiCo_2O_4$-Reduced Graphene Oxide Nanocomposites with Improved Electrochemical Poperties," *Electrochim. Acta*, vol. 141, pp. 126–133, 2014.

[78] M. Sun, Y. Dong, G. Zhang, J. Qu, and J. Li, "α-Fe_2O_3 Spherical Nanocrystals Supported on CNTs as Efficient Non-noble Electrocatalysts for the Oxygen Reduction Reaction," *J. Mater. Chem. A*, vol. 2, no. 33, pp. 13635–13640, 2014.

[79] Q. Tang, Z. Shan, L. Wang, and X. Qin, "MoO_2–Graphene Nanocomposite as Anode Material for Lithium-Ion Batteries," *Electrochim. Acta*, vol. 79, pp. 148–153, 2012.

[80] G. Xi, J. Ye, Q. Ma, N. Su, H. Bai, and C. Wang, "In Situ Growth of Metal Particles on 3D Urchin-like WO3 Nanostructures," *J. Am. Chem. Soc.*, vol. 134, no. 15, pp. 6508–6511, 2012.

[81] H. Chen, Y. Li, F. Zhang, G. Zhang, and X. Fan, "Graphene Supported Au-Pd Bimetallic Nanoparticles with Core-Shell Structures and Superior Peroxidase-like Activities," *J. Mater. Chem.*, vol. 21, no. 44, pp. 17658–17661, 2011.

[82] M. Sun, H. Liu, Y. Liu, J. Qu, and J. Li, "Graphene-Based Transition Metal Oxide Nanocomposites for the Oxygen Reduction Reaction," *Nanoscale*, vol. 7, no. 4, pp. 1250–1269, 2015.

[83] J. Chlistunoff, "RRDE and Voltammetric Study of ORR on Pyrolyzed Fe/Polyaniline Catalyst. On the Origins of Variable Tafel Slopes," *J. Phys. Chem. C*, vol. 115, no. 14, pp. 6496–6507, 2011.

[84] L. Cui, G. Lv, Z. Dou, and X. He, "Fabrication of Iron Phthalocyanine/Graphene Micro/Nanocomposite by Solvothermally Assisted π–π Assembling Method and its Application for Oxygen Reduction Reaction," *Electrochim. Acta*, vol. 106, pp. 272–278, 2013.

[85] C.-C. Chou, C.-H. Liu, and B.-H. Chen, "Effects of Reduction Temperature and pH Value of Polyol Process on Reduced Graphene Oxide Supported Pt Electrocatalysts for Oxygen Reduction Reaction," *Energy*, vol. 70, pp. 231–238, 2014.

[86] C. Du, Y. Sun, T. Shen, G. Yin, and J. Zhang, "7 - Applications of {RDE} and {RRDE} Methods in Oxygen Reduction Reaction," in *Rotating Electrode Methods and Oxygen Reduction Electrocatalysts*, W. X. Y. Zhang, Ed. Amsterdam: Elsevier, 2014, pp. 231–277.

[87] W. Il Park, C.-H. Lee, J. M. Lee, N.-J. Kim, and G.-C. Yi, "Inorganic Nanostructures Grown on Graphene Layers," *Nanoscale*, vol. 3, no. 9, pp. 3522–3533, 2011.

[88] L. De Rogatis, M. Cargnello, V. Gombac, B. Lorenzut, T. Montini, and P. Fornasiero, "Embedded Phases: A Way to Active and Stable Catalysts," *ChemSusChem*, vol. 3, no. 1, pp. 24–42, 2010.

[89] S. Cui, S. Mao, G. Lu, and J. Chen, "Graphene Coupled with Nanocrystals: Opportunities and Challenges for Energy and Sensing Applications," *J. Phys. Chem. Lett.*, vol. 4, no. 15, pp. 2441–2454, 2013.

[90] W. Sun, X. Wang, X. Sun, Y. Deng, J. Liu, B. Lei, and Z. Sun, "Simultaneous Electrochemical Determination of Guanosine and Adenosine with Graphene-ZrO_2 Nanocomposite Modified Carbon Ionic Liquid Electrode," *Biosens. Bioelectron.*, vol. 44, no. 1, pp. 146–151, 2013.

[91] C.-J. Cai, M.-W. Xu, S.-J. Bao, C. Lei, and D.-Z. Jia, "A Facile Route for Constructing a Graphene-Chitosan-ZrO_2 Composite for Direct Electron Transfer and Glucose Sensing," *RSC Adv.*, vol. 2, no. 21, p. 8172-8179, 2012.

[92] S. Guo, S. Zhang, and S. Sun, "Tuning Nanoparticle Catalysis for the Oxygen Reduction Reaction," *Angew. Chemie Int. Ed.*, vol. 52, no. 33, pp. 8526–8544, 2013.

[93] J. Xiao, Q. Kuang, S. Yang, F. Xiao, S. Wang, and L. Guo, "Surface Structure Dependent Electrocatalytic Activity of Co_3O_4 Anchored on Graphene Sheets toward Oxygen Reduction Reaction," *Sci. Rep.*, vol. 3:2300, 2013.

[94] Y. Zhang, F. Xu, Y. Sun, Y. Shi, Z. Wen, and Z. Li, "Assembly of $Ni(OH)_2$ Nanoplates on Reduced Graphene Oxide: A Two Dimensional Nanocomposite for Enzyme-Free Glucose Sensing," *J. Mater. Chem.*, vol. 21, no. 42, p. 16949-16954, 2011.

[95] Z. Wang, Y. Hu, W. Yang, M. Zhou, and X. Hu, "Facile One-Step Microwave-Assisted Route Towards Ni Nanospheres/Reduced Graphene Oxide Hybrids for Non-Enzymatic Glucose Sensing," *Sensors*, vol. 12, no. 4, pp. 4860–4869, 2012.

[96] S. Guo, S. Zhang, L. Wu, and S. Sun, "Co/CoO Nanoparticles Assembled on Graphene for Electrochemical Reduction of Oxygen," *Angew. Chemie – Int. Ed.*, vol. 51, no. 47, pp. 11770–11773, 2012.

[97] Q. He, Q. Li, S. Khene, X. Ren, F. E. López-Suárez, D. Lozano-Castelló, A. Bueno-López, and G. Wu, "High-Loading Cobalt Oxide Coupled with Nitrogen-Doped Graphene for Oxygen Reduction in Anion-Exchange-Membrane Alkaline Fuel Cells," *J. Phys. Chem. C*, vol. 117, no. 17, pp. 8697–8707, 2013.

[98] W.-H. Ryu, T.-H. Yoon, S. H. Song, S. Jeon, Y.-J. Park, and I.-D. Kim, "Bifunctional Composite Catalysts Using Co_3O_4 Nanofibers Immobilized on Nonoxidized Graphene Nanoflakes for High-Capacity and Long-Cycle Li–O_2 Batteries," *Nano Lett.*, vol. 13, no. 9, pp. 4190–4197, 2013.

[99] J. Feng, Y. Liang, H. Wang, Y. Li, B. Zhang, J. Zhou, J. Wang, T. Regier, and H. Dai, "Engineering Manganese Oxide/Nanocarbon Hybrid Materials for Oxygen Reduction Electrocatalysis," *Nano Res.*, vol. 5, no. 10, pp. 718–725, 2012.

[100] T. N. Lambert, D. J. Davis, W. Lu, S. J. Limmer, P. G. Kotula, A. Thuli, M. Hungate, G. Ruan, Z. Jin, and J. M. Tour, "Graphene-Ni-[small alpha]-MnO_2 and -Cu-[small alpha]-MnO_2 Nanowire Blends as Highly Active Non-Precious Metal Catalysts for the Oxygen Reduction Reaction," *Chem. Commun.*, vol. 48, no. 64, pp. 7931–7933, 2012.

[101] Y. Cao, Z. Wei, J. He, J. Zang, Q. Zhang, M. Zheng, and Q. Dong, "[small alpha]-MnO_2 Nanorods Grown In Situ on Graphene as Catalysts for Li-O_2 Batteries with Excellent Electrochemical Performance," *Energy Environ. Sci.*, vol. 5, no. 12, pp. 9765–9768, 2012.

[102] J. Zhang, C. Guo, L. Zhang, and C. M. Li, "Direct Growth of Flower-Like Manganese Oxide on Reduced Graphene Oxide Towards Efficient Oxygen Reduction Reaction," *Chem. Commun.*, vol. 49, no. 56, pp. 6334–6336, 2013.

[103] J. Duan, Y. Zheng, S. Chen, Y. Tang, M. Jaroniec, and S. Qiao, "Mesoporous Hybrid Material Composed of Mn_3O_4 Nanoparticles on Nitrogen-Doped Graphene for High-

ly Efficient Oxygen Reduction Reaction," *Chem. Commun.*, vol. 49, no. 70, pp. 7705–7707, 2013.

[104] J.-S. Lee, T. Lee, H.-K. Song, J. Cho, and B.-S. Kim, "Ionic Liquid Modified Graphene Nanosheets Anchoring Manganese Oxide Nanoparticles as Efficient Electrocatalysts for Zn-air Batteries," *Energy Environ. Sci.*, vol. 4, no. 10, pp. 4148–4154, 2011.

[105] J. Xiao, G. Xu, S.-G. Sun, and S. Yang, "MFe_2O_4 and MFe@Oxide Core–Shell Nanoparticles Anchored on N-Doped Graphene Sheets for Synergistically Enhancing Lithium Storage Performance and Electrocatalytic Activity for Oxygen Reduction Reactions," *Part. Part. Syst. Charact.*, vol. 30, no. 10, pp. 893–904, 2013.

[106] W. Zhang, Y. Zeng, C. Xu, H. Tan, W. Liu, J. Zhu, N. Xiao, H. H. Hng, J. Ma, H. E. Hoster, R. Yazami, and Q. Yan, "Fe_2O_3 Nanocluster-Decorated Graphene as O_2 Electrode for High Energy Li-O_2 Batteries," *RSC Adv.*, vol. 2, no. 22, pp. 8508–8514, 2012.

[107] R. Zhou, Y. Zheng, D. Hulicova-Jurcakova, and S. Z. Qiao, "Enhanced Electrochemical Catalytic Activity by Copper Oxide Grown on Nitrogen-Doped Reduced Graphene Oxide," *J. Mater. Chem. A*, vol. 1, no. 42, pp. 13179–13185, 2013.

[108] X.-Y. Yan, X.-L. Tong, Y.-F. Zhang, X.-D. Han, Y.-Y. Wang, G.-Q. Jin, Y. Qin, and X.-Y. Guo, "Cuprous Oxide Nanoparticles Dispersed on Reduced Graphene Oxide as an Efficient Electrocatalyst for Oxygen Reduction Reaction," *Chem. Commun.*, vol. 48, no. 13, pp. 1892–1894, 2012.

[109] H.-G. Jung, Y. S. Jeong, J.-B. Park, Y.-K. Sun, B. Scrosati, and Y. J. Lee, "Ruthenium-Based Electrocatalysts Supported on Reduced Graphene Oxide for Lithium-Air Batteries," *ACS Nano*, vol. 7, no. 4, pp. 3532–3539, 2013.

[110] Y. Li, L. Zhang, Z. Hu, and J. C. Yu, "Synthesis of 3D Structured Graphene as a High Performance Catalyst Support for Methanol Electro-Oxidation," *Nanoscale*, vol. 7, no. 25, pp. 10896–10902, 2015.

[111] D. Deng, X. Pan, L. Yu, Y. Cui, Y. Jiang, J. Qi, W.-X. Li, Q. Fu, X. Ma, Q. Xue, G. Sun, and X. Bao, "Toward N-Doped Graphene via Solvothermal Synthesis," *Chem. Mater.*, vol. 23, no. 5, pp. 1188–1193, Mar. 2011.

[112] X. Feng, Y. Zhang, J. Zhou, Y. Li, S. Chen, L. Zhang, Y. Ma, L. Wang, and X. Yan, "Three-Dimensional Nitrogen-Doped Graphene as an Ultrasensitive Electrochemical Sensor for the Detection of Dopamine," *Nanoscale*, vol. 7, no. 6, pp. 2427–2432, 2015.

[113] H. M. Jeong, J. W. Lee, W. H. Shin, Y. J. Choi, H. J. Shin, J. K. Kang, and J. W. Choi, "Nitrogen-Doped Graphene for High-Performance Ultracapacitors and the Importance of Nitrogen-Doped Sites at Basal Planes," *Nano Lett.*, vol. 11, no. 6, pp. 2472–2477, Jun. 2011.

[114] H. Wang, T. Maiyalagan, and X. Wang, "Review on Recent Progress in Nitrogen-Doped Graphene: Synthesis, Characterization, and Its Potential Applications," *ACS Catal.*, vol. 2, no. 5, pp. 781–794, May 2012.

[115] S. Yang, L. Zhi, K. Tang, X. Feng, J. Maier, and K. Müllen, "Efficient Synthesis of Heteroatom (N or S)-Doped Graphene Based on Ultrathin Graphene Oxide-Porous Silica Sheets for Oxygen Reduction Reactions," *Adv. Funct. Mater.*, vol. 22, no. 17, pp. 3634–3640, 2012.

[116] J. Li, X. Li, P. Zhao, D. Y. Lei, W. Li, J. Bai, Z. Ren, and X. Xu, "Searching for Magnetism in Pyrrolic N-Doped Graphene Synthesized via Hydrothermal Reaction," *Carbon*, vol. 84, pp. 460–468, Apr. 2015.

[117] W. Zhou, J. Zhou, Y. Zhou, J. Lu, K. Zhou, L. Yang, Z. Tang, L. Li, and S. Chen, "N-Doped Carbon-Wrapped Cobalt Nanoparticles on N-Doped Graphene Nanosheets for High-Efficiency Hydrogen Production," *Chem. Mater.*, vol. 27, no. 6, pp. 2026–2032, Mar. 2015.

[118] Z.-H. Sheng, L. Shao, J.-J. Chen, W.-J. Bao, F.-B. Wang, and X.-H. Xia, "Catalyst-Free Synthesis of Nitrogen-Doped Graphene via Thermal Annealing Graphite Oxide with Melamine and Its Excellent Electrocatalysis," *ACS Nano*, vol. 5, no. 6, pp. 4350–4358, Jun. 2011.

[119] Z. Yang, Z. Yao, G. Li, G. Fang, H. Nie, Z. Liu, X. Zhou, X. Chen, and S. Huang, "Sulfur-Doped Graphene as an Efficient Metal-free Cathode Catalyst for Oxygen Reduction," *ACS Nano*, vol. 6, no. 1, pp. 205–211, Jan. 2012.

[120] S. Bag, B. Mondal, A. K. Das, and C. R. Raj, "Nitrogen and Sulfur Dual-Doped Reduced Graphene Oxide: Synergistic Effect of Dopants Towards Oxygen Reduction Reaction," *Electrochim. Acta*, vol. 163, no. 0, pp. 16–23, 2015.

IntechOpen